Introducing the physics of quasi-one-dimensional organic conductors

C. Bourbonnais[1]

Département de Physique, Université de Sherbrooke, Québec, Canada

[1]Based on the lectures given at the *Boulder School for Condensed Matter and Materials Physics, Strongly Correlated Materials*, University of Colorado, Boulder, June 30-July 18, 2008.

Contents

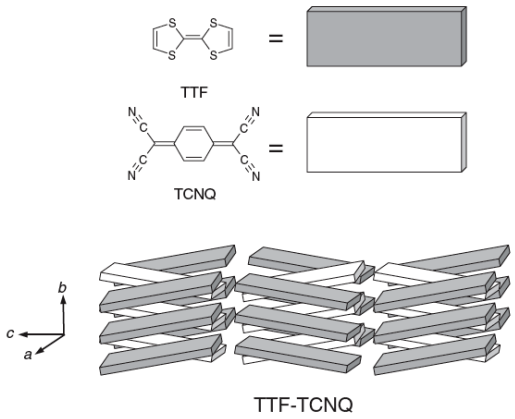

FIGURE 1. Molecular constituents and crystal structure of TTF-TCNQ, after [4].

1 Quasi-one-dimensional molecular conductors : what are they ?

In most situations organic molecules retain their planar shape in the solid state and a frequent type of packing is the chain like motif, where the intermolecular interaction is the strongest along the chain direction. Such face to face overlap of the π molecular orbitals leads to a one-dimensional electron band formation. However, the orbital overlap transverse to the stacking direction, albeit much smaller, does exist so that these stacks are in practice coupled and best visualized as close realizations of one-dimensional systems – commonly called quasi-one-dimensional (quasi-1D) molecular materials. Most stable molecular entities used so far have their highest occupied molecular orbital (HOMO) completely filled and as such would be band insulators. Moreover, the lowest unoccupied molecular orbital (LUMO) is in general too far in energy to have a chance to overlap with the HOMO for the formation of a semi-metal.[2] Metallic behavior is usually achieved by combining two different molecular species in the synthesis, *viz.,* two organic molecules as in two-chain charge transfer salts or an organic molecule with an inorganic radical as in cation radical salts. Thus good electron donors and acceptors in the solid state yield the possibility of electron charge transfer from one specie to the other. The overlap of partly filled molecular shells then leads to a partly filled electron bands, a prerequisite to metallic properties.

2 The first organic quasi-one-dimensional metal: TTF-TCNQ

The first stable organic metal is the celebrated two-chain charge transfer salt TTF-TCNQ (tetrathiofulvalinium -tetracyanoquinodimethane). It is formed by the combination of a good electron acceptor, the TCNQ molecule synthesized at the beginning of the sixties,[2] and a good electron donor, the TTF molecule whose synthesis was stimulated by F. Wudl about ten years later [3]. Crystals of TTF-TCNQ consist of segregated stacks of $TTF^{+\delta}$ and $TCNQ^{-\delta}$ (Fig. 1); the charge transfer, which can be determined by X-ray diffuse scattering, is $\delta \approx 0.59$e per molecule. The hole (TTF) and electron (TCNQ) bands are then incommensurate. From a one-electron point of view , TTF-TCNQ should be a metal, which is indeed found experimentally over a large temperature interval with a conductivity parallel to the chains $\sigma_{\|} \sim 500(\Omega \cdot \mathrm{cm})^{-1}$ at ambient temperature reaching $10^4 ... 10^{-5}(\Omega \cdot \mathrm{cm})^{-1}$ down to 60 K. The ratio of parallel and perpendicular conductivities is in the range $\sigma_{\|}/\sigma_{\perp} \sim 10^2 \ldots 10^3$ at ambient temperature which confirms the quasi-one dimensional anisotropy of this materials alluded before.

The chain conductivity of TTF-TCNQ reaches a pronounced peak at $T_P \simeq 59$K, below which the system (to be more precise the TCNQ chains) undergoes a metal insulator transition (Fig. 2) This low temperature gap opening at the Fermi level turns out to be the common fate of many quasi-1D organic (and inorganic as well) metals. Actually, it is a remarkable consequence of the so-called *Peierls mechanism* for the formation of a coupled electron-lattice superstructure at the wave vector $2k_F$ that is twice the Fermi wave vector k_F. According to the Peierls prediction made in 1955[6]: a one-dimensional metallic state is never stable at zero temperature against

[2]Although recent attempts to realize a a semi-metallic system, the $Ni(tmdt)_2$, from the HOMO-LUMO overlap within a single component molecular crystal have been successful [1].

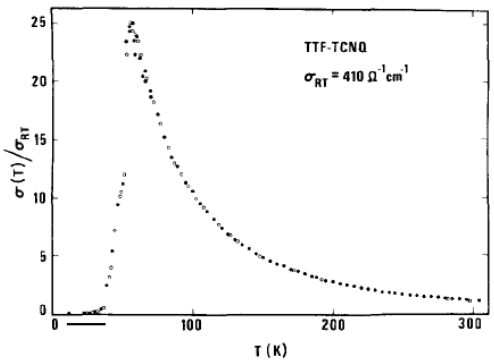

FIGURE 2. DC conductivity along the chains for TTF-TCNQ. Taken from Ref. [5].

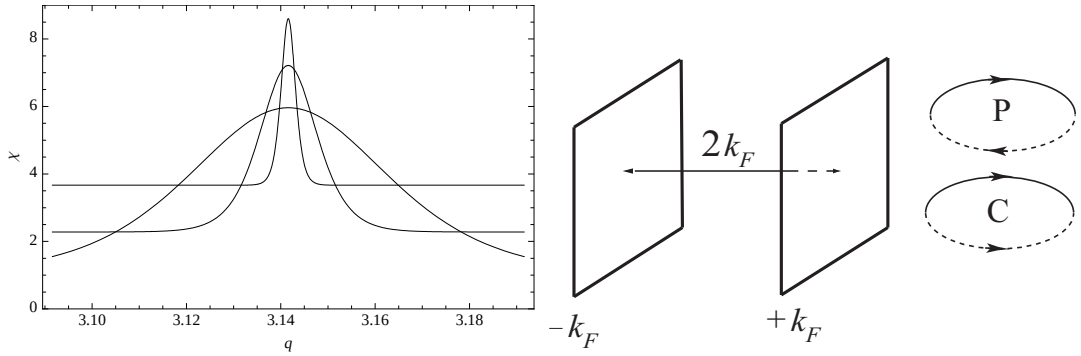

FIGURE 3. Free electron density response $\chi^0(q,T)$ as a function of the wave vector q and for different temperatures. A logarithmic singularity due to perfect nesting develops at $q = 2k_F$ $(= \pi)$ as the temperature is lowered (left); A similar singularity is also found for the Cooper pairing response $\chi^0_C(q = 0, T)$ at zero momentum pair $q = 0$. One dimensional Fermi planes connected by the nesting vector $2k_F$ (middle). The diagrammatic representation of the Peierls (P) and Cooper (C) free responses (right). The continuous (dashed) line refers to a particle near $+k_F(-k_F)$.

the formation of a $2k_F$ superstructure and the opening of a gap at the Fermi level.

2.1 The Peierls instability of a one-dimensional metal

The Peierls instability against the formation of a one-dimensional superstructure takes its origin in the singular response of a one-dimensional *free* electron gas in the formation of a $2k_F$ – charge or spin – density-wave. It takes the form of a logarithmic singularity in the density-density (Lindhard) response function of non interacting electrons at the wave vector $q = 2k_F$, which takes the form

$$\chi^0_P(q,T) = \frac{1}{\pi}\int dk\, \frac{n(\epsilon_k) - n(\epsilon_{k+q})}{\epsilon_{k+q} - \epsilon_k} \tag{1.1}$$

where $n(x) = 1/(e^{x/T} + 1)$ and

$$\epsilon_k = -2t\cos ka \tag{1.2}$$

is the tight binding electron spectrum, with t as the hopping integral along the chain axis. A key property that enters in the evaluation of the $\chi^0(2k_F, T)$ is the electron-hole symmetry of the spectrum, namely

$$\epsilon_k = -\epsilon_{k+2k_F}, \tag{1.3}$$

which is called 'nesting' between electron and hole separated by $2k_F$ (Fig. 3). The fact that this relation can be realized by a macroscopic number of k states is responsible of the singularitiy. The explicit evaluation of χ^0_P at low temperature yields

$$\chi^0_P(q,T) = N(0)\Big[\ln\frac{1.13E_F}{T} - \psi\Big(\frac{1}{2}\Big) + \Re\mathrm{e}\,\psi\Big(\frac{1}{2} + \frac{iv_F(q-2k_F)}{4\pi T}\Big)\Big], \tag{1.4}$$

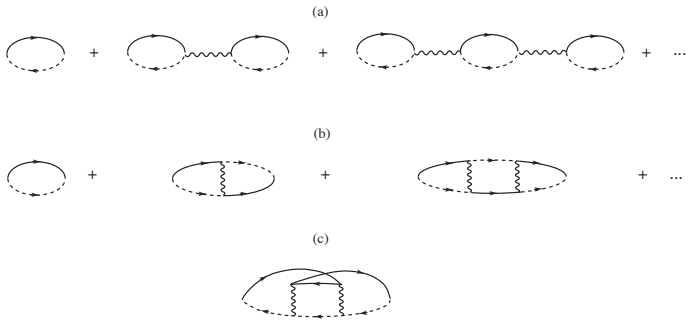

FIGURE 4. (a): Leading diagrammatic (ladder) series of the CDW susceptibility near $2k_F$; (b) Ladder series for the singlet superconducting susceptibility; (c) Example of interference term between the Peierls and Cooper scattering channels for the CDW susceptibility.

derived in the low temperature domain $E_F \ll T$, where $E_F = v_F k_F$ is the Fermi energy, $v_F = 2t$, the Fermi velocity and $k_F = \pi/2$ (taken here for simplicity at half-filling). Here $\psi(x)$ is the diGamma function and $N(0) = 1/(\pi v_F)$ is the density of states at the Fermi level. As shown in the Fig. 3, χ_P^0 develops a logarithmic divergence at $q = 2k_F$ as $T \to 0$.

The singular behavior of χ_P^0 is the driving force behind the Peierls instability. In effect, the lattice vibrations, which modulate the electronic overlap t, couple to the electron density response and can produce an instability of the metallic state against the formation of a Peierls superstructure at finite temperature. In a weak coupling picture of the electron-phonon interaction, this can be readily seen by considering the following Hamiltonian describing the linear coupling of electrons to phonons in a one-dimensional system of length L

$$H = \sum_{k,\sigma} \epsilon_k \, c^\dagger_{k,\sigma} c_{k,\sigma} + \sum_q \omega_q b^\dagger_q b_q + \frac{g}{\sqrt{L}} \sum_{k,q,\sigma} c^\dagger_{k+q,\sigma} c_{k,\sigma} \big(b^\dagger_q + b_{-q} \big), \tag{1.5}$$

where $c^{(\dagger)}_{k,\sigma}$ is the destruction (creation) operator for electron of wave vector k and spin σ, and $b^{(\dagger)}_q$ for acoustic phonons of wave vector q with the spectrum $\omega_q = \omega_D |\sin qa/2|$, where ω_D is the Debye energy at $2k_F$. Electrons are coupled to phonons through the linear interaction g, which is assumed to be momentum independent for k close to the Fermi level and momentum transfer q near $2k_F$.

Treating the electron-phonon term in perturbation theory, the leading corrections to the electronic Peierls susceptibility can be expressed in terms of a geometric – RPA – series of close loops

$$\begin{aligned} \chi_P(q,T) &= \chi_P^0(q,T) + \chi_P^0(q,T)\lambda\chi_P^0(q,T) + \chi_P^0(q,T)\lambda\chi_P^0(q,T)\lambda\chi_P^0(q,T) + \dots \\ &= \frac{\chi_P^0(q,T)}{1 - \lambda\chi_P^0(q,T)}, \end{aligned} \tag{1.6}$$

where $\lambda = g^2/\omega_D$. The series is represented diagrammatically in Fig. 4. It has a simple pole structure, which according to the singularity in χ_P^0 due to nesting, develops a divergence at the finite 'critical temperature'

$$T_P^0 = 1.13 E_F \, e^{-1/\tilde{\lambda}}. \tag{1.7}$$

An infinitesimal electron-phonon coupling at $2k_F$ is thus sufficient to create an instability of the metallic state against the formation of a $2k_F$ charge-density-wave superstructure. Below T_P^0, the growing static superstructure opens a gap Δ in the electron spectrum at the Fermi level, which coincides with the (real) order parameter at half-filling. For incommensurate band fillings, however, the $2k_F$ wave vector of CDW has no commensurate relation with the underlying lattice; the order parameter then becomes complex, $\Delta = |\Delta| \, e^{i\phi}$, and acquires besides the amplitude gap $|\Delta|$, a collective phase ϕ degree of freedom that allows the CDW to move collectively under the influence of an electric field and 'superconducts'. This is the so-called Frölich mode for the conductivity.

In the above crude approach, which is equivalent to a mean-field theory, it should be stressed that T_P^0 cannot be squared with a true critical temperature. Actually one-dimensional systems cannot sustain long-range order at finite temperature for an electron-phonon interaction like Eq.(1.5), because of fluctuation effects, which confine correlations to short distances. Nevertheless, T_P^0 remains a meaningful temperature scale for the onset of the

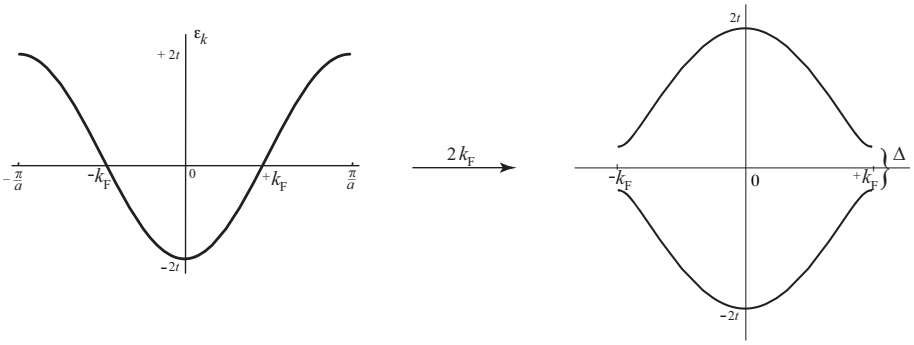

FIGURE 5. Formation of the Peierls gap at the Fermi level in the presence of a $2k_F$ superstructure.

precursors of the transition that usually takes place at a sizably lower temperature, as a consequence of a finite but small interchain coupling that makes the system effectively three-dimensional at sufficiently low temperature[3].

One-dimensional precursors to the Peierls transition are indeed systematically observed from X-ray diffuse scattering experiments, showing the existence of diffuse lines of scattering, which is symptomatic of 1D short-range CDW correlations over a large temperature intervals.

The relevance of the electron-phonon interaction for the occurrence of the Peierls mechanism raises naturally the question as to why it does not also favor superconductivity as for ordinary superconductors in three dimensions ? Electron-electron or Cooper pairing was completely neglected in the above perturbation theory which focuses exclusively on electron-hole pairing (Fig. 4-a). This was done despite the fact that the Cooper response to singlet (or triplet) pairing for free electrons, which will be noted $\chi_C(q,T)$, is well known to show the same logarithmic singularity at zero pair momentum q, that is

$$\begin{aligned}\chi_C^0(q,T) &= \frac{1}{\pi}\int dk\,\frac{n(-\epsilon_k)-n(\epsilon_{-k+q})}{\epsilon_{-k+q}+\epsilon_k} \\ &= N(0)\Big[\ln\frac{1.13E_F}{T}-\psi\Big(\frac{1}{2}\Big)+\Re\mathrm{e}\,\psi\Big(\frac{1}{2}+\frac{iv_Fq}{4\pi T}\Big)\Big]. \end{aligned} \tag{1.8}$$

This singularity is a direct consequence of a different symmetry, a kind of 'nesting', but now for pairs of electron (or hole) states in the spectrum

$$\epsilon_k = \epsilon_{-k}, \tag{1.9}$$

which holds in any spatial dimension. Following the example of the BCS theory of ordinary superconductors in isotropic systems, we can write down a perturbation expansion for the Cooper pairing response in the presence of phonons near $2k_F$. At the lowest – ladder – level, one gets the diagrammatic series of Fig. 4-b. At variance with the closed loop summation in the Peierls case, all the internal Cooper loops are open with a phonon exchange that involves an intermediate phonon frequency sum. The summation is strongly dependent on retardation which is fixed by the scale $\omega_D \ll E_F$ of phonons, much smaller than the Fermi energy scale. Retardation then lowers the cut-off of the Cooper singularity from E_F to ω_D with the result for the singlet superconducting response

$$\chi_C(q=0,T) = \frac{\chi_C^0(T)}{1-\frac{1}{2}\tilde{\lambda}\ln\frac{1.13\omega_D}{T}}. \tag{1.10}$$

This leads to the familiar BCS result

$$T_C^0 = 1.13\omega_D\, e^{-2/\tilde{\lambda}}, \tag{1.11}$$

for the temperature scale of the singlet pairing instability. The comparison with the Peierls scale T_P^0 in Eq. (1.7) indicates that strong retardation in the electron-phonon interaction, that is $\omega_D \ll E_F$, is detrimental to superconductivity. This is an important factor explaining why the Peierls instability is often encountered in quasi-one-dimensional metals.

[3]For a three-dimensional Peierls ordered state, interchain coupling can originate from many sources. Interchain Coulomb interaction between CDW, three-dimensional phonons and interchain single electron hopping can each or together assure the occurrence of a true phase transition at finite temperature $T_P \ll T_P^0$.

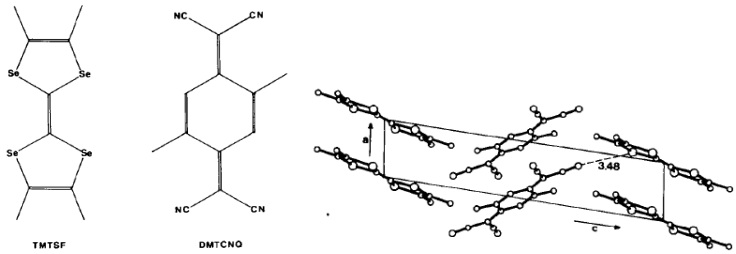

FIGURE 6. Donnor (TMTSF) and acceptor (DMTCNQ) molecules (left); crystal structure of)TMTSF-DMTCNQ. After Ref. [10]

When retardation in the interaction is suppressed, namely when $\omega_D \sim E_F$, as it is the case for the coupling to higher energetic phonon (e.g. intramolecular) modes[4] or for the direct non retarded Coulomb repulsive term, the Peierls and Cooper instabilities enter in a subtle – quantum mechanical – competition. Both pairing channels interfere with and distort each other to all order in the perturbation theory of the scattering amplitudes (see e.g. Fig.1.6 -c); this either totally or the at the best partly invalidates the separate scattering channel approximation developed above. The outcome of this quantum interference for the ground state is in general neither a classical Peierls state nor a BCS superconductor, but a quantum liquid of a different nature. The so-called *Luttinger and Luther-Emery* liquids enter in this category and will play an important part in the description of other organic charge transfer salts.

3 TMTSF-DMTCNQ: the pivotal compound in the discovery of organic superconductivity

It was soon recognized that the Peierls instability is a stumbling block to the existence of superconductivity in the low-dimensional organic conductors. How to weaken, nay suppress the underlying driving force of this structural instability was an important goal of both physicists and chemists in the second half of the seventies. Nesting, at the core of the Peierls mechanism, has to be altered. By virtue of Eq.(1.3), an effective alteration can be attained by considering higher dimensional effects in the electronic band structure, which have been neglected so far. It was early shown that a finite single-electron hopping between nearest-neighbor chains $t_\perp$ can indeed introduce small but finite perfect nesting deviations that can suppress the logarithmic singularity at sufficiently low temperature [8]. The enhancement of inter stack kinetic coupling was an important stimulus for chemistry in the synthesis of new molecules with an enhanced transverse molecular overlap in the solid state. On the physics side, hydrostatic pressure was found to be a tool *par excellence* to increase the molecular overlap in these loosely packed compounds. The ambient incommensurate Peierls compound TTF-TCNQ was one of the compounds for which a large range of pressure has been applied [9, 4] (Fig.7) . Although the complete suppression of the Peierls state has been shown very recently to be virtually achieved at a pressure as high as 80kbar [4], no superconductivity is found yet.

It turned out that the combination of chemistry and experimental physics proved to be a key determinant in the success that followed. The first breakthrough came near the end of seventies with the synthesis by Bechgaard *et al.,* [10, 11] of the two-chain compound TMTSF-DMTCNQ based on the donor molecule TMTSF (tetramethylselenafulvalene)[12]. It is born on the donor side of the parent molecule TTF by substituting sulfur (S) with selenium (Se), and each corner hydrogen (H) with methyl group (CH_3) (Fig. 8); and from the modified donor TCNQ molecule, the DMTCNQ[5]. The crystal structure consists of planes of TMTSF and DMTCNQ stacks Fig. 6. The charge transfer for TMTSF-DMTCNQ is $\delta = 0.5$e per molecule as determined by X-ray measurements; this leads to a three-quater filled (commensurate) band for TMTSF stacks with close inter stack contacts between selenium atoms and presumably better transverse electronic overlap. The electronic properties of this compound are essentially dominated by the TMTSF stacks as a result of the addition of the methyl groups on the

[4]The coupling to intramolecular (Einstein) modes are present in practice but usually found to be relatively small (see for example Ref. [7]).

[5]DMTCNQ (dimethyltetracyanoquinodimethane) is obtained from TCNQ by substituting two H with CH_3 on each side of the carbon ring at the center.

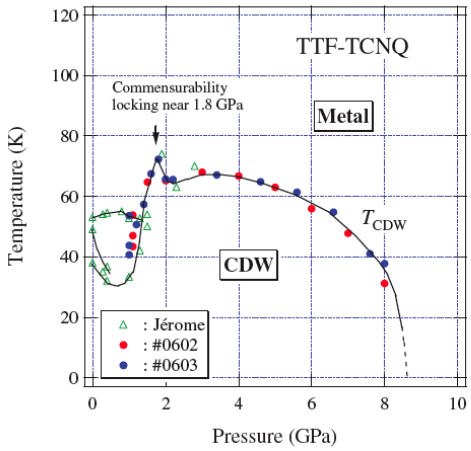

FIGURE 7. Variation of the Peierls critical temperature as a function of pressure in TTF-TCNQ. After refs. [9, 4]

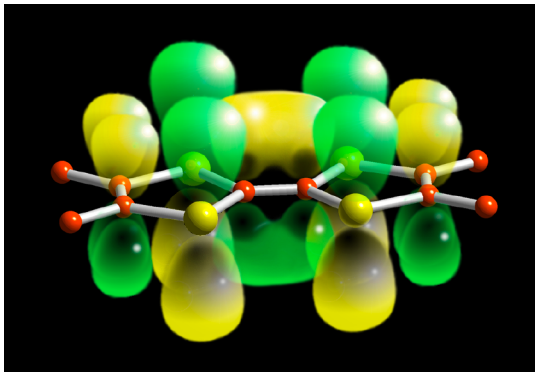

FIGURE 8. TMTSF donor molecule with the profile of atomic orbitals that enter in the HOMO. The cousin sulfur based molecule TMTTF has a similar form.

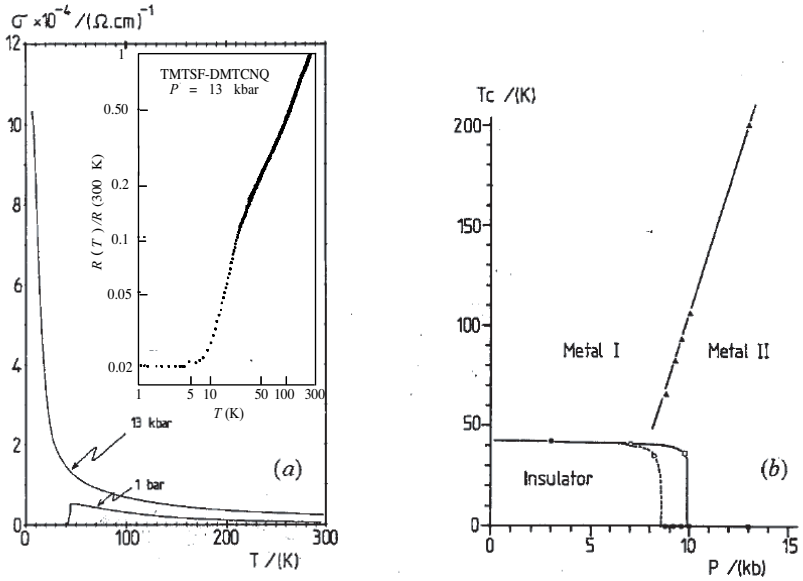

FIGURE 9. TMTSF-DMTCNQ: (a) parallel conductivity *vs* temperature at 1 bar and 13 kbar (inset: normalized longitudinal resistivity *vs* T at 13 kbar) ; (b) Temperature *vs* Pressure phase diagram; the metal I and metal II lines refer to the temperature scale where the interchain electron motion becomes coherent. After[14].

acceptor molecule which produces a steric factor that sizably reduces the intra-stack overlap along the DMTCNQ chains. Longitudinal electric transport already showed a pronounced metallic behavior at ambient temperature which continues down to 40K, where it is followed by a sharp metal-insulator transition. The Peierls character of the transition was confirmed by X-ray diffuse scattering [13]. As shown by Andrieux *et al.* from the Jerome's group in Orsay [14], however, the Peierls insulating state is quite sensitive to pressure and becomes entirely suppressed under 13 kbar (Fig. 9). A highly conducting state is then stabilized down to the lowest temperature. TMTSF-DMTCNQ under pressure stands out as the first stable highly conducting organic metal below the helium temperature.

Frustration of nesting due to an increase of dimensionality is a consequence of the wrapping of the Fermi surface which is proportional to the electronic overlap energy $t_\perp$. As temperature $T < t_\perp$, the warping is no longer blurred by thermal fluctuations and transverse one-electron band motion becomes coherent and then sensitive to departure from perfect nesting electrons. These deviations can come from small corrections to the electron spectrum. Let us add one additional dimension and consider the following spectrum of the quasi-1D case

$$\epsilon_k \to E(\mathbf{k}) = \epsilon_k - 2t_\perp \cos(k_\perp) - 2t_{\perp 2}\cos(2k_\perp). \tag{1.12}$$

where $t_\perp$ and $t_{\perp 2}$ are the hoppings amplitudes between the first and the second nearest-neighbor chains, and for which $t_{\perp 2} \ll t_\perp$. Deviations from perfect nesting at the two-dimensional wave vector $\mathbf{q}_0 = (2k_F, \pi)$ comes the small corrections due to the second harmonic term $t_{\perp 2}$. This can be seen from the relation for nesting at $\mathbf{q_0}$, which becomes

$$E(\mathbf{k}+\mathbf{q}_0) = -E(\mathbf{k}+\mathbf{q}_0) + 4t_{\perp 2}\cos 2k_\perp \tag{1.13}$$

where $\mathbf{k} = (k, k_\perp)$. Using this two-dimensional spectrum $E(\mathbf{k})$, the free electron CDW susceptibility at $\mathbf{q}_0$ is modified and now reads

$$\chi^0(\mathbf{q}_0, T) = N(0)\Big\{ \ln(1.13E_F/T) + \psi\Big(\frac{1}{2}\Big) - \Big\langle \psi\Big(\frac{1}{2} - i\frac{t_{\perp 2}\cos 2k_\perp}{\pi T}\Big)\Big\rangle_{k_\perp}\Big\} \tag{1.14}$$

where $\langle \ldots \rangle_{k_\perp}$ is a $k_\perp$ average over the transverse Brillouin zone. The presence of $t_{\perp 2}$ begins to lower the amplitude of the susceptibility at the temperature scale $T \sim t_{\perp 2}$, which is followed by the complete suppression of the divergence at $T \ll t_{\perp 2}$. Thus from the replacement of Eq. (1.14) in (1.6), the equation for T_P becomes

$$\ln\frac{T_P}{T_P^0} = \psi\Big(\frac{1}{2}\Big) - \Big\langle \psi\Big(\frac{1}{2} - i\frac{t_{\perp 2}\cos 2k_\perp}{\pi T_P}\Big)\Big\rangle_{k_\perp}. \tag{1.15}$$

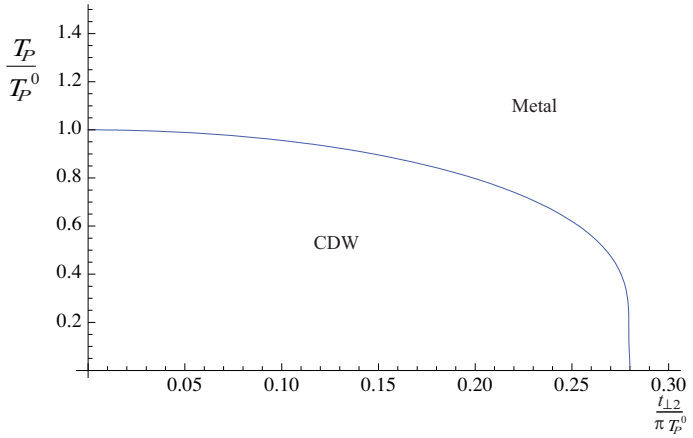

FIGURE 10. Variation of the normalized Peierls mean-field critical temperature as the nesting deviations parameter $t_{\perp 2}$. A similar variation can be found in the RPA treatment of the Metal-SDW transition for a wrapped Fermi surface with nesting deviations (see text).

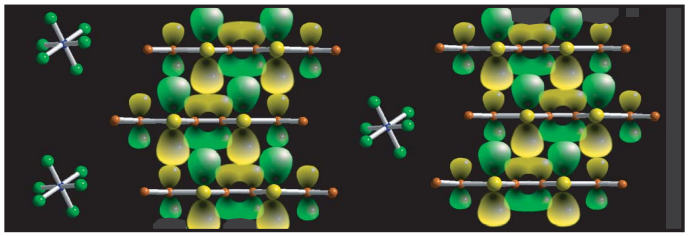

FIGURE 11. Side view of the crystal structure of the Bechgaard (and Fabre) salts $(TMTSF)_2X$ [$(TMTTF)_2X$] series.

The solution leads to the Peierls temperature as a function of nesting deviations is shown in Fig. 10. Comparing with Fig.9-b, nesting frustration can mimic the pressure dependence and can then provide a reasonable mechanism for the suppression of the Peierls instability.

4 The Bechgaard and Fabre salts series

4.1 The Bechgaard salts

While TMTSF-DMTCNQ did not show superconductivity up to 13 kbar, its stable metallic state gave the necessary impetus for chemistry to further explore the synthesis of materials based on the promising TMTSF molecule. So at nearly the end of 1979, Bechgaard *et al.*[15], introduced a new series of one-chain cation radial salts, the $(TMTSF)_2X$, where the choice of the small inorganic (radical) ion X= PF_6^-, AsF_6^-, NO_3^-, ..., leads to a series of isostructural compounds, soon christened as the *Bechgaard salts series* (Fig. 11). The zig-zag stacking of the TMTSF molecules creates cavities for the anions which together with the triclinic structure favors a slight dimerization of the organic stacks. At ambient pressure the metallic character is well marked at room temperature and for compounds like X= PF_6^- and AsF_6^- with centro-symmetrical anions, it carries on for temperature as low as 12K or so where a sharp metal-insulator transition occurs – the case of $(TMTSF)_2PF_6$ is shown in Fig. 12.

Initially believed as a Peierls phase transition, X-ray experiments fail to detect any lattice superstructure [13]. The insulating state was quickly found to be the result of a magnetic superstructure, a spin-density-wave (SDW) state. The SDW state will be discussed in more details below. In parallel pressure studies were undertaken on the $(TMTSF)_2PF_6$ compound by Jerome *et al.,* at Orsay [17]; the insulating state was found to be rapidly suppressed and ultimately giving rise to superconductivity at $T_c = 0.9$K under 12 kbar of pressure (Fig. 13). The zero field phase diagram of the first organic superconductor $(TMTSF)_2PF_6$ is shown in Fig. 14. A comparable phase diagram was found for $(TMTSF)_2AsF_6$ with a similar centro-symmetrical anion [18]. Substituting PF_6 with the non centrosymmetrical anion ClO_4 yielded first ambient pressure organic superconductor $(TMTSF)_2ClO_4$ below

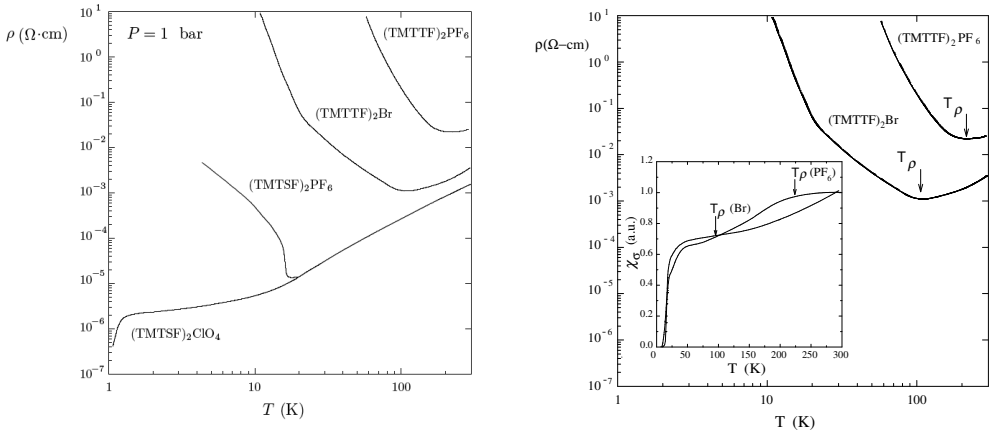

FIGURE 12. Resistivity *vs* temperature of selected members of the Bechgaard and Fabre salts series at ambient pressure (left), after [15]; Resistivity and spin susceptibility *vs* temperature for members of the Fabre series, showing the decoupling of charge and spin degrees of freedom at the temperaure scale T_ρ for the Mott localization (right), taken from [16]

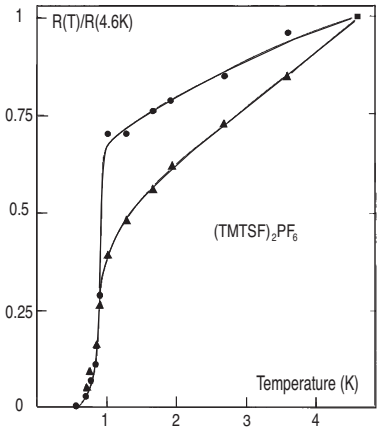

FIGURE 13. The first organic superconductor $(TMTSF)_2PF_6$: original resistivity data (on two different samples) under 12 kbar of pressure, after Jerome *et al.*, [17].

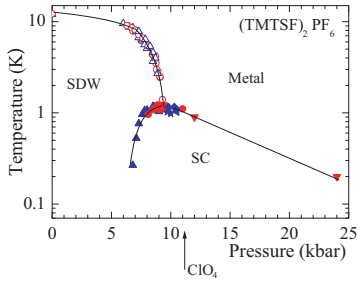

FIGURE 14. Critical temperature *vs* pressure phase diagram of $(TMTSF)_2PF_6$. The arrow corresponds to the effective location of the ambient pressure superconductor $(TMTSF)_2ClO_4$ on the pressure axis. Courtesy of P. Auban-Senzier (2008).

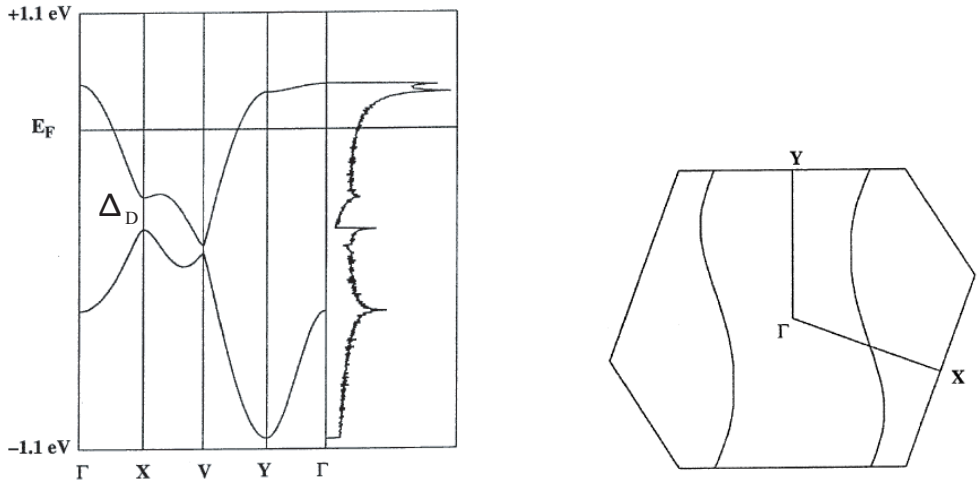

FIGURE 15. Electronic band structure of $(TMTSF)_2X$ compounds for the Highest Occupied Molecular Orbital (HOMO) and the corresponding open Fermi surface as obtained from extended Huckel calculations. Here the small dimerization of the stack introduces a dimerization gap Δ_D in the middle of a 3/4 filled band making the band effectively half-filled. After[20].

FIGURE 16. RPA ladder approximation for the SDW magnetic response at $\mathbf{q}_0$. The coupling g^* stands for the effective Coulomb interaction in the temperature regime where the warping of the Fermi surface is coherent.

$T_c \simeq 1.2$K [19] (Fig. 12). This shows that by anion substitution, discrete moves along the pressure axis can be carried out as a chemical pressure effect (Fig. 14).

The fact that superconductivity can be stabilized in the very close proximity of SDW or itinerant antiferromagnetic state puzzled almost everybody in the field. The phase diagram constituted the first striking example – well before the coming of H-T_c cuprates ! – of antiferromagnetism adjacent to the emergence of superconductivity. It turns out that antiferromagnetism completely surrounds superconductivity in these materials, not only along the pressure axis, but also along the magnetic field **H** axis where the destruction of the superconducting phase is quickly followed by a cascade of field-induced SDW states when $\mathbf{H} \| c^*$, namely oriented in a particular direction perpendicular to the chains. Since the presence of a SDW state, as itinerant antiferromagnetism, indicates that *repulsive Coulomb interaction* dominates in this material. This in turn is symptomatic of an unconventional mechanism for superconductivity that would be at play and the requirements for a traditional phonon-mediated mechanism for (singlet) Cooper pairing are not met.

Suppression of the spin-density-wave state of $(TMTSF)_2X$ under pressure. – If we disregard for a moment the existence of superconductivity in $(TMTSF)_2X$, the rapid suppression of the SDW state at the approach of the critical pressure P_c bears some similarity with the CDW case for TMTSF-DMTCNQ (Fig. 9). Although the Coulomb repulsion is a necessary ingredient for SDW, nesting at the best nesting wave vector $\mathbf{q}_0$ of the open Fermi surface remains the driving force of the magnetic instability. Following the example of the CDW, one can look at an RPA approach to the SDW instability by considering the RPA summation of Figure 16. The result is

$$\chi_{SDW}(\mathbf{q}_0, T) \propto \frac{\chi^{0*}(\mathbf{q}_0, T)}{1 - \frac{1}{2} g^* \chi^{0*}(\mathbf{q}_0, T)}, \tag{1.16}$$

where the effective elementary susceptibility in presence of nesting deviation is given by

$$\chi^{0*}(\mathbf{q}_0, T) = N(0) \Big\{ \ln(1.13 E_x/T) + \psi\Big(\frac{1}{2}\Big) - \Big\langle \psi\Big(\frac{1}{2} - i\frac{t_{\perp 2} \cos 2k_\perp}{\pi T}\Big)\Big\rangle_{k_\perp} \Big\}. \tag{1.17}$$

Here the only difference with CDW [Eq. (1.14)] is the cut-off $E_x \sim t_\perp$, which here differs from E_F. This is so because for non-retarded interaction like the Coulomb term, the RPA approach is, as we will see in § 5.4,

meaningless above the hopping scale $t_\perp$ for the coherence of the wrapping of the Fermi surface and it is only below E_x, that the single scattering channel approximation recovers some validity. As for the electron-electron coupling g^*, it values does not coincide with the bare interaction but rather with an effective or renormalized coupling that includes non RPA corrections above the (crossover) scale E_x, where the electron system is essentially one-dimensional.

In complete analogy with the CDW case, the singularity of $\chi_{SDW}(\mathbf{q}_0, T)$ at $T = T_{SDW}$ is given by the equation

$$\ln \frac{T_{SDW}}{T^0_{SDW}} = \psi\Big(\frac{1}{2}\Big) - \Big\langle \psi\Big(\frac{1}{2} - i\frac{t_{\perp 2}\cos 2k_\perp}{\pi T_P}\Big)\Big\rangle_{k_\perp}. \tag{1.18}$$

which follows a variation as a function of $t_{\perp 2}$ that is identical to the one of Fig. 10, and which qualitatively bears some ressemblance with the experimental situation. We will see in § 5.4 how to use the renormalization group method to go beyond RPA and include residual quantum interference between Cooper and Peierls pairings and thus treating SDW and superconductivity on the same footing.

4.2 The Fabre salts and the universal phase diagram of (TM)$_2$X

From an historical point of view the TMTSF organic molecule was preceded by the synthesis by Fabre *et al.* of the TMTTF molecule [21], another offshoot of the parent molecule TTF. TMTTF was obtained by substituting each corner carbon of TTF with a methyl group; the molecule is isomorphous to its selenium counterpart shown in Fig. 8. A variety of one-chain cation radical salts (TMTTF)$_2$X, now known as the *Fabre salts*, were synthesized prior to the Bechgaard salts. Both families of compounds are isostructural (Fig. 11), the (TMTTF)$_2$X showing, however, a more pronounced dimerization of the stacks in normal pressure conditions. For a given X, a (TMTTF)$_2$X S-S interstack distances are longer than the corresponding Se-Se in (TMTSF)$_2$X, an early indication for weaker interchain orbital overlap in (TMTTF)$_2$X [22].

Although the (TMTTF)$_2$X salts in normal pressure conditions were all found to be insulating at relatively high temperature, they show a very rich phase diagram that is closely related to the one of Bechgaard salts. The peculiar sequence of both non ordered and ordered states found in these materials, as a function of either pressure or anion substitution, complements and even overlap with the sequence found in (TMTSF)$_2$X series. Both series then form an impressive unity.

Let us single out some of its important features. First consider the non ordered phase of the two compounds (TMTTF)$_2$PF$_6$ and (TMTTF)$_2$Br. From the temperature dependent resistivity curves shown in the right part of Fig. 12, both compounds become insulating below $T_\rho \simeq$ 220K and 100K, respectively [23]. According to X-ray, these anomalies are not associated to any lattice superstructure. Moreover, the uniform susceptibility measurements, which probe spin degrees of freedom, show a gapless behavior and is uninfluenced by what is going on in the charge sector of both materials (inset of Fig. 12). This contrasts with an ordinary band semiconducting behavior where both conductivity and susceptibility show an activated temperature behavior. Spin and charge degrees of freedom are here apparently, a characteristic of a Mott insulating state produced by strong electron repulsion for a half-filled band. Comparing the gap $\Delta_\rho(\sim 2T_\rho)$ with interchain hopping parameter $t_\perp \approx 100$K obtained by band calculations for (TMTTF)$_2$X [24], we realize that the insulating state occurs in a temperature range where the warping of the Fermi surface is incoherent and the compoundss are essentially one-dimensional. The one-dimensional character of the Mott state is further revealed by the smooth crossover like behavior at T_ρ.

The insulating state below T_ρ distinguishes itself by a sequence of phase transitions and long-range orders. In (TMTTF)$_2$PF$_6$ for example, the spin degrees of freedom become first gapped below $T_{SP} \approx 19K$. X-ray experiments have shown that the transition is accompanied by new Bragg spots indicative of a static superstructure at the wave vector $(2k_F, \pi, \pi)$. Since $T_{SP} \ll T_\rho$, the transition occurs deeply in the insulating state where the charge degrees of freedom are strongly localized. Therefore the superstructure is not the consequence of a Peierls transition but rather of a *spin-Peierls* instability. Under pressure both T_ρ and $T_{\rm SP}$ decrease, and at some critical pressure $P_0 \sim$ 9kbar, $T_{\rm SP}$ dips sharply towards zero. Beyond P_0 on the pressure axis, the nature of the ground state then changes completely becoming antiferromagnetic with a Néel ordered state below a temperature T_N that increases rapidly with pressure [16]. The critical pressure where both T_{SP} and T_N points towards zero can be seen as a quantum critical point [25]. The antiferomagnetic state of (TMTTF)$_2$PF$_6$ around 10kbar $> P_0$, is quite similar to the ordered state of (TMTTF)$_2$Br salt with a $T_N \approx$ 15K at ambient pressure. Therefore substituting PF$_6$ with Br is virtually equivalent to a shift of the origin of the pressure axis. This equivalence is consistent with

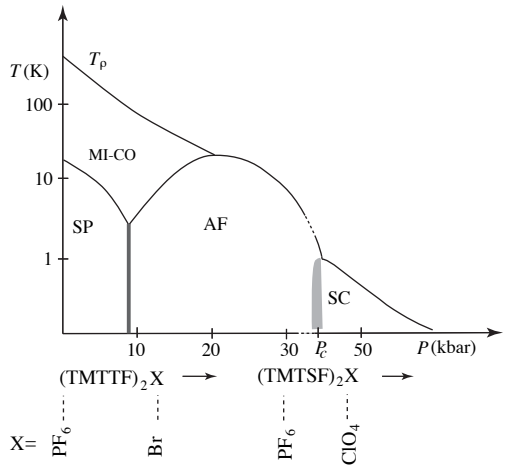

FIGURE 17. Generic phase diagram of the $(TMTTF)_2X$ and $(TMTSF)_2X$ as a function of pressure and anion X substitution. MI stands for Mott insulating, CO for charge ordered state, SP stands for spin-Peierls, AF for antiferromagnetism, SC for superconductivity.

the fact that pressure is likely to reduce stack dimerization and improve interchain S-S contacts of $(TMTTF)_2PF_6$ close to the values found for the Bromine salt.

The Mott scale T_ρ for $(TMTTF)_2Br$ is progressively suppressed while its T_N increases under pressure. The latter reaches a maximum value of 23 K or so near 5 kbar [26], where T_ρ merges with the critical domain associated to the transition and becomes an irrelevant scale beyond the maximum. The high temperature phase is then completely metallic down to the transition which is still antiferromagnetic but rather refers to an itinerant antiferromagnet or a SDW state. A similar Néel - SDW passage is found for $(TMTTF)_2PF_6$ but around 15 kbar with a maximum of $T_N \approx 20$K. At that point the physics of members of the Fabre series becomes in many respects similar to the one the Bechgaard salts. At sufficiently high pressure the SDW state can indeed be completely suppressed and superconductivity stabilized above a critical pressure P_c, which is compound dependent ! Until now, superconductivity has been found in $(TMTTF)_2Br$ (P_c = 26kbar) [27], $(TMTTF)_2PF_6$ ($P_c = 45$ kbar) [28, 29], $(TMTTF)_2AsF_6$ (P_c = 45 kbar) [30], $(TMTTF)_2SbF_6$ (P_c = 54 kbar) [31], and $(TMTTF)_2BF_4$ ($P_c = 33.5$ kbar)[32, 33]. The generic phase diagram of both series, termed $(TM)_2X$, is shown in Fig. 17.

5 The quasi-one-dimensional electron gas model

In this section we shall introduce some results of the scaling theory of the so-called electron gas model, whose properties are rather generic of what may happen in the phase diagram of $(TM)_2X$.

5.1 One dimensional results and connections with the normal phase of $(TMTTF)_2X$

Given the pronounced one-dimensional anisotropy of the compounds, it is natural to first consider the 1D limit of this model. To this end, we have seen above that the study of susceptibilities of non interacting electrons is particularly revealing of the natural infrared singular singularities for Peierls and Cooper pairing responses in one dimension.

As mentioned above what thus really makes one dimension electron systems so peculiar resides in the fact that both singularities refer to the same set of electronic states and will then interfere one another [34]. In the presence of non retarded weak interactions like the Coulomb term, the Cooper-Peierls interference is found to all order of perturbation theory for the scattering amplitudes of electrons with opposite Fermi velocities. The interference modifies the nature of the electron system in a essential way. In the framework of the 1D electron gas model, these infrared singularities put a selected emphasis on electronic states close to the Fermi level, which allows us to define various possible interactions with respect to the Fermi points $\pm k_F$ [35, 36]. Thus for a rotationally

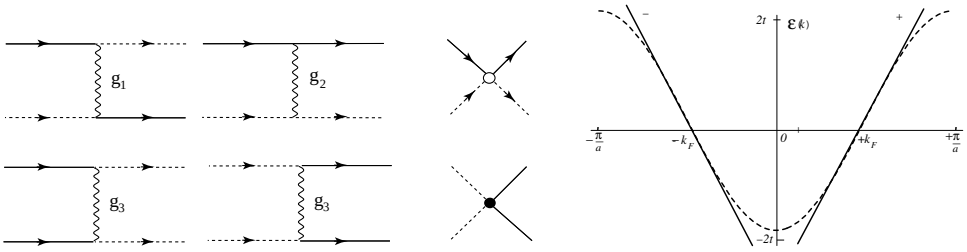

FIGURE 18. Backward (g_1), forward (g_2) and umklapp (g_3) couplings of the 1-D fermion gas model and the corresponding diagrams (left); The open (full) circle corresponds to the generic vertex part for backward and forward (umklapp) scatterings (middle); linear spectrum of the model (right).

invariant system of length L, the Hamiltonian of the electron gas model can be written in the form

$$\begin{aligned} H &= \sum_{k,p,\sigma} \epsilon_p(k) c^\dagger_{p,k,\sigma} c_{p,k,\sigma} \\ &+ \frac{1}{L} \sum_{\{k,q,\sigma\}} g_1 \; c^\dagger_{+,k_1+2k_F+q,\sigma} c^\dagger_{-,k_2-2k_F-q,\sigma'} c_{+,k_2,\sigma'} c_{-,k_1,\sigma} \\ &+ \frac{1}{L} \sum_{\{k,q,\sigma\}} g_2 \; c^\dagger_{+,k_1+q,\sigma} c^\dagger_{-,k_2-q,\sigma'} c_{-,k_2,\sigma'} c_{+,k_1,\sigma} \\ &+ \frac{1}{2L} \sum_{\{p,k,q,\sigma\}} g_3 \; c^\dagger_{p,k_1+p2k_F+q,\sigma} c^\dagger_{p,k_2-p2k_F-q+pG,\sigma'} c_{-p,k_2,\sigma'} c_{-p,k_1,\sigma}, \end{aligned} \tag{1.19}$$

where $\epsilon_p(k) \simeq v_F(pk - k_F)$ is the electron spectrum energy after a linearization close to right ($pk_F = +k_F$) and left ($pk_F = -k_F$) Fermi points; g_1 and g_2 are the backward and forward scattering amplitudes, respectively, whereas g_3 corresponds to Umklapp scattering, a process made possible at half-filling where the reciprocal lattice vector $G = 4k_F = 2\pi/a$ enters in the momentum conservation law. However, owing to the existence of a small dimerization gap $\Delta_D \ll E_F$ of organic stacks of $(TM)_2X$ (See Fig. 15), only weak half-filled Umklapp scattering $g_3 \approx g_1\Delta_D/E_F$ is present [37, 38]. Note that lattice models in their continuum limit can be mapped on the electron gas (continuum) model. In the Hubbard case, for example, the couplings $g_1 = g_2 = U$ coincide with the one-site Coulomb term U.

In the one-loop perturbation theory, the electron scattering amplitudes $g_{i=1,2,3}$ are corrected by the aforementioned Cooper and Peierls logarithmic singularities. These logarithms are scale invariant quantities as a function of energy or temperature, which allow us to write down scaling or renormalization group (RG) flow equations for the various $g_{i=1,2,3}$. This can be done according to different techniques [36, 39, 40, 41, 42]. We will adopt here the so-called Kadanoff-Wilson scheme [41, 42], which has been summarized in the Appendix. After all cancellations between Cooper and Peierls terms due to interference, the remaining terms allow us to write down flow equations of the coupling constants as a function of the energy distance from the Fermi level

$$\begin{aligned} \tilde{g}_1' &= -\tilde{g}_1^2 + \dots \\ (2\tilde{g}_2' - \tilde{g}_1') &= \tilde{g}_3^2 + \dots \\ \tilde{g}_3' &= \tilde{g}_3(2\tilde{g}_2 - \tilde{g}_1) + \dots, \end{aligned} \tag{1.20}$$

where $\tilde{g}_i' = \partial_\ell \tilde{g}_i$. Here ℓ is the logarithmic – loop – variable; it is related to the energy distance $\frac{1}{2}E_0 e^{-\ell} = E_F e^{-\ell}$ from the Fermi level, where E_0 is the band width. The long wavelength spin excitations are governed by the $\tilde{g}_1 \equiv g_1/\pi v_F$ coupling, whose flow, according to (1.20), is decoupled from both $\tilde{g}_3 \equiv g_3/\pi v_F$ and the combination $2\tilde{g}_2 - \tilde{g}_1 \equiv (2g_2 - g_1)/\pi v_F$ connected to charge excitations. In the physically relevant repulsive sector for systems like $(TM)_2X$ where $g_{1,2} > 0$, $g_1 - 2g_2 <\mid g_3 \mid$, the integration of Eqs.(1.20) shows that both $2g_2 - g_1$ and g_3 are relevant variables for the charge and scale to the strong coupling sector, where a charge gap Δ_ρ is found below the temperature scale $T_\rho(\sim \Delta_\rho/2)$. In one dimension, T_ρ does no refer to a true phase transition but merely to a crossover to a charge localization at wave vector $4k_F$.

Since Umklapp scattering leads to momentum dissipation, it contributes to the electrical resistivity. From the imaginary part of the one-particle self-energy in lowest order [43, 40], the electron-electron contribution to

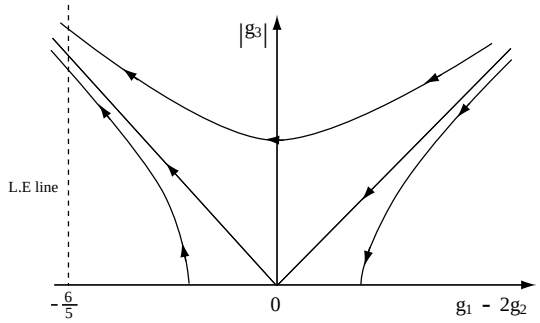

FIGURE 19. Flow of coupling constants as a function of ℓ in the charge sector. The weakly dimerized compounds $(TM)_2X$ have a small g_3 and repulsive $g_1 \sim g_2 > 0$ ($g_1 - 2g_2 < 0$) and would be located below the separatrix on left hand side of the diagram; there g_3 is relevant and crosses the Luther-Emery line where an exact solution can be found using the bosonzation method.

electrical resistivity can be deduced as a function of g_3 in one dimension

$$\rho(T) \propto T g_3^2(T). \tag{1.21}$$

Thus as a relevant coupling the growth of g_3 is responsible for an increase of resistivity towards the Mott insulating (MI) state. In the MI state elaborate calculations give rise to an exponential increase of resistivity [40].

On the other hand, in the spin sector the solution $\tilde{g}_1(T) = \tilde{g}_1/(1 + \tilde{g}_1 \ln E_F/T)$ for the g_1 coupling, which follows from Eq. (1.20), is marginally irrelevant and scales to zero, leaving the spins degrees of freedom gapless as shown by the calculation of the uniform spin susceptibility[44, 35],

$$\chi_\sigma(T) = \frac{2\mu_B^2(\pi v_\sigma)^{-1}}{1 - \frac{1}{2}\tilde{g}_1(T)}. \tag{1.22}$$

If $g_1(T)$ is decreasing as a function of temperature, then the spin susceptibility will decrease smoothly as a function of temperature. Most importantly if $g_1(T)$ is decoupled from the other – charge coupling – it will be unaffected by the occurrence of a charge gap. This decoupling is consistent with transport and susceptibility data shown in Fig.12.

The observed pressure effect on T_ρ can also be qualitatively understood from the above 1D scaling equations. In effect under pressure the amplitude of the stack dimerization and then the bare amplitude of g_3 are reduced. This defers ℓ_ρ for strong coupling in g_3 and $2g_2 - g_1$ to larger values. T_ρ is then progressively decreasing under pressure. Anion X substitution leads to a similar (chemical) pressure effect (see e.g. Fig.12).

When interaction are repulsive the electron system develops singularities for some staggered density-wave response. Thus the $2k_F$ SDW or antiferromagnetic response, which is governed by the combination of couplings $\tilde{g}_2(\ell) + \tilde{g}_3(\ell)$ that flows to strong coupling, develops a power law singularity of the form

$$\chi_{\rm AF}(2k_F, T) \propto (\pi v_F)^{-1}(T/\Delta_\rho)^{-\gamma}, \tag{1.23}$$

where the power law exponent $\gamma = \tilde{g}_2(T_\rho) + \tilde{g}_3(T_\rho) \sim 1$. The response for the $2k_F$ 'bond-centered' charge-density-wave, also called the bond-order-wave (BOW) response, which is governed by the combination of couplings $\tilde{g}_2(\ell) + \tilde{g}_3(\ell) - 2\tilde{g}_1(\ell)$, also develops a power law singularity in temperature

$$\chi_{\rm BOW}(2k_F, T) \propto (\pi v_F)^{-1}(T/\Delta_\rho)^{-\gamma_{\rm BOW}}. \tag{1.24}$$

Here the exponent $\gamma_{\rm BOW} \sim 1$ is essentially the same as the one of AF response – the amplitude of the latter being larger, however [45]. As we will see when $2k_F$ phonons are included, their coupling to singular BOW correlations yields a lattice instability of the spin-Peierls (SP) type. It is then interesting to note that the most singular responses AF and BOW, and a finite Mott gap Δ_ρ in the phase diagram of the repulsive 1D electron gas model the observed phase diagram of $(TMTTF)_2X$ (Fig. 20).

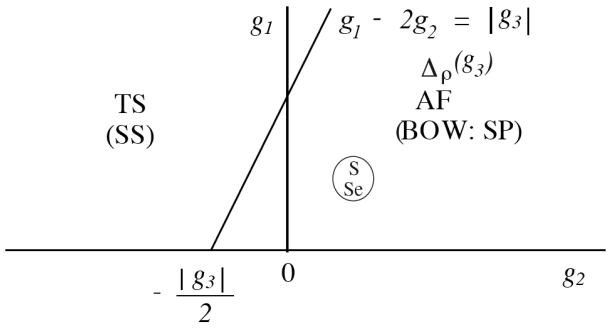

FIGURE 20. Phase diagram of the one-dimensional electron gas model at $g_1 > 0$. $(TM)_2X$ are likely to be located in the repulsive sector where the antiferromagnetic (AF) and the bond-order-wave (BOW) response functions are the most singular in the presence of a Mott gap Δ_ρ; also shown the attractive sector where Umklapp is irrelevant and where triplet (TS) and singlet (SS) superconducting responses are singular.

5.2 Electronic confinement

In the presence of interchain hopping $t_\perp$, the parameter space of the model is enlarged and becomes for the initial action

$$\mu_S = (G_p^0(k,\omega_n), t_\perp, g_1, g_2, g_3) \tag{1.25}$$

The renormalization group transformation given by Eq. (57) in the Appendix, when carried out beyond the one-loop level, not only alters the scattering amplitudes g_i but also the single-particle propagator [41]. At sufficiently high energy, the corresponding one-particle self-energy corrections keep in first approximation their 1D character and then modify the purely one-dimensional part of the propagator through the renormalization factor $z(\ell)$. Thus the effective quasi-1D propagator at step ℓ reads

$$\begin{aligned} G_p(\mathbf{k},\omega_n,\mu_S(\ell)) &= \frac{1}{z(\ell)[G_p^0(k,\omega_n)]^{-1} + 2t_\perp \cos k_\perp} \\ &= \frac{z(\ell)}{i\omega_n - \epsilon_p(k) + 2z(\ell)t_\perp \cos k_\perp}. \end{aligned} \tag{1.26}$$

Detailed calculations show that $z(\ell)$ obeys a distinct flow equation at the two-loop level which depends on the couplings constants [41]. Its integration up to ℓ_T shows that $z(T)$ follows a power law in temperature

$$z(T) \sim \left(\frac{T}{E_F}\right)^\theta, \tag{1.27}$$

where the exponent $\theta = \mathcal{O}(g^2) > 0$. Being the residue at the single-particle pole of the 1D propagator, $z(T)$ coincides with the reduction factor of the density of states at the Fermi level . The reduction of the density of states along the chains also modifies the amplitude of interchain hopping, that is $t_\perp \to z t_\perp$. Consequently the temperature T_x at which the warping of the Fermi surface becomes coherent and electrons deconfine will be renormalized downward. Deconfinement occurs when $T_x \sim z(T_x)t_\perp$ or

$$T_x \sim t_\perp \left(\frac{t_\perp}{E_F}\right)^{(1-\theta)/\theta}. \tag{1.28}$$

According to this expression, T_x decreases when the interaction − which can be parametrized by the exponent θ − increases; it is non-zero as long as $\theta < 1$ for which $t_\perp$ remains a relevant variable. The system then undegoes a crossover to the formation of quasi-particles in a Fermi liquid with the quasi-particle weight $z(T_x)$. For strong coupling, T_x vanishes at the critical value $\theta_c = 1$ and becomes undefined for $\theta > 1$, $t_\perp$ being then marginal in the former case and irrelevant in the latter Consequently, in the latter case, no transverse band motion is possible and the single-particle coherence is spatially confined along the stacks. Large value $\theta \sim 1$ are found on the Luther-Emery line at half-filling in the presence of a charge gap [39, 46]. Therefore a visible gap Δ_ρ for $(TMTTF)_2X$ implies that $t_\perp$ is irrelevant and T_x cannot take place. At low pressure, $(TMTTF)_2X$ are then said to be *electronic confined* with no possibility to form a Fermi liquid [47].

5.3 The Néel order of (TMTTF)$_2$X series

The question then now arises whether $t_\perp$, as an irrelevant one-particle process, can nevertheless promote long-range antiferromagnetic order. Actually, this possibility exists and results from *interchain pair-hopping* processes. These are not present in the Hamiltonian at the start but emerge when interactions along the stacks combine with $t_\perp$ in the one-dimensional region[41, 42].

For repulsive interactions, the most important pair hopping contribution is the *interchain exchange* which favors antiferromagnetic ordering of neighboring chains. Roughly speaking, from each partial trace operation in (44), there is a 'seed' $f(\ell)d\ell$ of interchain exchange that builds up as a result of combining perturbatively the effective hopping $(zt_\perp)$ and the couplings $(g's)$ in the shell of degrees of freedom to be integrated out. This can be seen as a new relevant interaction for the system, which in its turn is magnified by antiferromagnetic correlations. The net interchain exchange term generated by the flow of renormalization can be written as

$$S_\perp = -\frac{1}{4}\sum_{\langle i,j\rangle}\sum_{\widetilde{q}} J_\perp(\ell)\,\mathbf{S}_i(\widetilde{q})\cdot\mathbf{S}_j(\widetilde{q}), \tag{1.29}$$

which favors antiferromagnetic of spins on neighboring chains i and j. Going to transverse Fourier space, $J_\perp$ corresponds to the exchange amplitude at the ordering wave vector $\mathbf{Q}_0 = (2k_F, \pi)$. In the one-dimensional regime, it is governed at the one-loop level by the distinct flow equation

$$\frac{d}{d\ell}\tilde{J}_\perp = f(\ell) + \tilde{J}_\perp\gamma(\ell) + \frac{1}{2}(\tilde{J}_\perp)^2, \tag{1.30}$$

where $\tilde{f}(\ell) \simeq 2[(\tilde{g}_2(\ell)+\tilde{g}_3(\ell))t_\perp/E_0]^2 e^{(2-2\theta(\ell))\ell}$. Here $\theta(\ell)$ and $\gamma(\ell)$ are the power law exponents of the one-particle propagator (Eq. (1.27)) and antiferromagnetic response (Eq. (1.23)) respectively.

One distinguishes two different situations. The first one corresponds to the presence of a charge gap well above the transition as it occurs for (TMTTF)$_2$X. We have seen earlier that it defines a domain of ℓ where $\theta(\ell)$ is large and $\gamma(\ell) = 1$, that is $2 - 2\theta(\ell) - \gamma(\ell) < 0$. The physics of this strong coupling regime bears some resemblance to the problem of weakly coupled Heisenberg spin chains. However, in the Luther-Emery liquid case with a smaller gap $\Delta_\rho \ll E_F$ each electron is not confined to a single site as in the Heisenberg limit but is delocalized over a finite distance $\xi_\rho \sim v_F/\Delta_\rho$, corresponding to the size of bound electron-hole pairs. A simple analysis of (1.30) shows that for $T \ll \Delta_\rho$, $J_\perp$ takes the transverse RPA form

$$J_\perp(\mathbf{Q}_0, T) \propto \frac{J_\perp^0}{1 - J_\perp^0\chi_{\rm AF}(2k_F, T)} \tag{1.31}$$

where $J_\perp^0 \approx \pi\xi_\rho(t_\perp^{*2}/\Delta_\rho)$ is an effective antiferromagnetic interchain exchange coupling over the distance ξ_ρ. When coupled to singular correlations along the chains, this leads to the antiferromagnetic transition temperature

$$T_N \approx \frac{t_\perp^{*2}}{\Delta_\rho}, \tag{1.32}$$

where $t_\perp^* = z(\Delta_\rho)t_\perp$ is the one-particle hopping at the energy scale of the charge gap.

A characteristic feature of strong coupling is the *increase* of T_N when the gap Δ_ρ *decreases* (Fig. 21). The increase continues up to the point where $T_N \sim T_\rho$; there the insulating behavior resulting from the charge gap merges into the critical domain of the transition. θ and γ then take smaller weak coupling values in the normal metallic domain so that $2 - 2\theta(\ell) - \gamma(\ell)$ will first reach zero after which it will become positive corresponding to interchain pair-hopping in weak coupling. In this second situation, the growth of the seed term surpasses the second one due to pair vertex corrections in (1.30). An approximate expression of the transition temperature in this case is found to be

$$T_c \approx g^{*2}t_\perp^*, \tag{1.33}$$

where $g^* = g_2^* + g_3^*$ and $t_\perp^* = t_\perp z(T_c)$. This expression makes sense as long as $T_c > T_x$, which on the scale of interaction should not correspond to a wide interval. In the latter there is a decrease of T_c for decreasing interactions. This leads to a *maximum* of T_c at the boundary between strong and weak coupling domains (Fig. 21).

As soon as $T_c < T_x$, the single particle deconfinement occurs first at $zt_\perp \approx E_0(\ell)$ and interchain hopping can no longer be treated as a perturbation. and this invalidates (1.30). We have have seen earlier that a Fermi

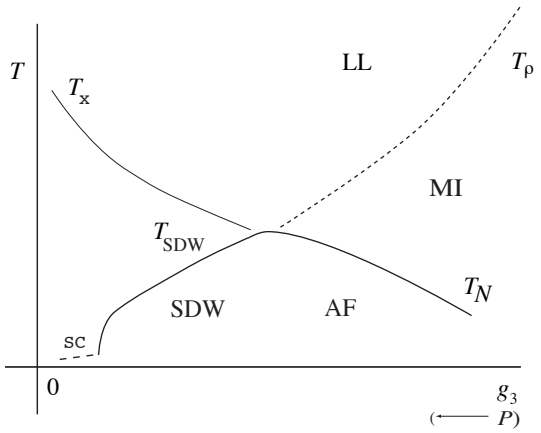

FIGURE 21. Qualitative sketch of the temperature scale of the calculated phase diagram by the renormalization group method. After Refs. [42, 58, 56].

liquid component forms under these conditions. An instability towards SDW is still possible under good nesting conditions for the *entire Fermi surface*. This situation corresponds roughly to the one treated earlier in the single channel approximation to the SDW and CDW (Peierls) instabilities.

5.4 On the origin of organic superconductivity in (TM)$_2$X

While the simple RPA approach given above can account for the rapid suppression of the SDW phase under pressure, it is restricted to electron-hole pairing channel and tells nothing about how superconductivity can be possible. At the microscopic level electron-hole pairs at $(\mathbf{k}, \mathbf{k} \pm \mathbf{q}_0)$ will coexist with electron-electron (and hole-hole) pairing at $(\mathbf{k}, -\mathbf{k})$ and this connects once again to the problem of interfering pairing instabilities. At finite $t_{\perp b}$ and for temperature well below $T^\star$, however, the outcome differs from purely one dimension and may provide a logical link between SDW and superconductivity.

The connection between superconductivity and density-wave correlations in isotropic systems goes back to the work of Kohn and Luttinger in the mid sixties [48]. They showed that the coupling between electron-hole (density-wave) and electron-electron correlations, albeit very small, is still present for a spherical Fermi surface. In this isotropic limit, $2k_F$ Friedel (charge) fluctuations act as a oscillating pairing potential for electrons giving rise to a purely electronic mechanism for superconductivity at large angular momentum. Emery suggested that this non-phonon mechanism should be working in the spin sector as well, being boosted by the proximity of a SDW state in the quasi-1D geometry in order to yield experimentally reachable T_c [49] – an effect that was early on confirmed in the framework of renormalized mean-field theory [50, 51, 52] and various RPA approaches [53, 54, 55]. However, these approaches amount to extract an effective superconducting coupling from short-range density-wave correlations, which in turn serves as the input of a ladder diagrammatic summation similar to the one given in Fig. 1.6-b . It turns out that the ladder theory, as a single channel approximation, neglects the quantum interference between the different kinds of pairings, and as such it cannot capture the dynamical emergence of superconductivity.

Because of the finite value of $t_\perp$, interference becomes *non uniform* along the Fermi surface. This non uniformity generates a momentum dependence in the scattering amplitudes, which can be parametrized by the set of transverse wave vectors for in going $(k_{\perp 1} k_{\perp 2})$ and outgoing $(k'_{\perp 1} k'_{\perp 2})$ electrons. The generalization of the 1D scaling equations Eqs. (1.20) to now $k_\perp$-dependent interactions $g_{i=1,2,3}(k'_{\perp 1} k'_{\perp 2} k_{\perp 2} k_{\perp 1})$ in the quasi-1D case, where both $t_\perp$ and $'_{\perp 2}$ are present, has been worked out recently [56, 57, 58, 59]. The results can be put in the following schematic form:

$$\partial_\ell g_i(k'_{\perp 1} k'_{\perp 2} k_{\perp 2} k_{\perp 1}) \qquad = \sum_{k_\perp} \sum_{n,n'=1}^{3} \Big\{ \epsilon^{nn'}_{C,i}\, g_n(\{k_\perp\})\, g_{n'}(\{k_\perp\}) \mathcal{L}'_C(k_\perp, q_{C\perp})$$

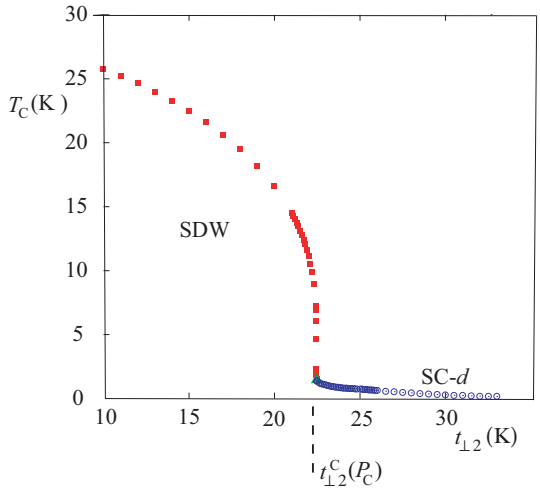

FIGURE 22. Calculated phase transition temperature of the quasi-one-dimensional electron gas model as a function of the nesting deviation parameter $t_{\perp 2}$ for repulsive intrachain interactions $g_{1,2,3}$. After Nickel *et al.,* Ref. [56, 57]

$$+\,\epsilon_{P,i}^{nn'}\, g_n(\{k_\perp\})\, g_{n'}(\{k_\perp\})\mathcal{L}'_P(k_\perp, q_{P\perp}, t'_{\perp b})\Big\}, \tag{1.34}$$

Here $\mathcal{L}'_{C,P} = \partial_\ell \mathcal{L}_{C,P}$ where $\mathcal{L}_{C,P}$ are the Cooper (electron-electron) and Peierls (electron-hole) loops, with $q_{C,P\perp}$ as their respective $\{k_\perp\}$-dependent transverse momentum variables, and $\epsilon_{C,P,i}^{nn'} = \pm 1$, or 0. By integrating these flow equations, the singularities shown by interactions signal instabilities of the normal state at a critical temperature T_c. The nature of ordering is determined by the profile of interactions in $\{k_\perp\}$ space, which in turn corresponds to a divergence of a given order parameter susceptibility χ_μ. Feeding these equations with a realistic set of bare parameters for the repulsive intrachain interactions g_i and the band parameters $t_\perp$ and E_F in $(TM)_2X$, it is possible to follow the instabilities of the normal state as a function of the nesting deviations parameter $t_{\perp 2}$, which simulates the main influence of pressure in the model [56, 57, 58, 59, 60].

Thus at perfect nesting, when $t_{\perp 2} = 0$, the normal state develops an SDW instability at $T_c^0 \sim 20$K, which for small Umklapp scattering corresponds to the range of T_c expected in most of $(TMTSF)_2X$ at ambient pressure and $(TMTTF)_2X$ at relatively high pressure. The range of T_c roughly squares with the one obtained in the single channel approximation with no interference below T_x discussed above. As $t_{\perp 2}$ increases, T_c is gradually decreasing until the critical range $t'^{\rm cr}_{\perp 2} \sim T_c^0$ is reached where the SDW is suppressed (Fig. 22). The metallic phase remains unstable at finite temperature, however, but the instability now takes place in the superconducting channel (bleu symbols, Fig. 22). The order parameter is of the form $\Delta(k_\perp) = \Delta \cos k_\perp$ and has nodes at $k_\perp \pm \pi/2$; it corresponds to a interstack singlet or $d_{x^2-y^2}$-wave pairing. Therefore for repulsive intrachain interactions, an attraction between electrons can be dynamically generated from the interference between Cooper and Peierls scattering channels. The attraction between carriers on neighboring chains can be seen as being mediated by spin fluctuations. The fact that SCd and SDW instability lines meet at the maximum of the superconducting $T_c \sim 1$K and that the ratio $T_c^0(\text{SC}d)/T_c^0(\text{SDW}) \sim 1/20$, together with their respective $t'_\perp$ dependence are worth noticing features in regard to the experimental phase diagram (Fig. 14).

Regarding the possible symmetries of the superconducting order parameter, an analysis of the momentum dependence of the scattering amplitude $g_i(\{k_\perp\})$ reveals that for the electron gas model defined with only *intra*chain repulsive interactions, the strongest superconducting instability is invariably found in the singlet SCd-wave channel [58, 60]. Triplet superconductivity in the p_x channel, which has been proposed on phenomenological grounds as a possible candidate to describe superconductivity in the Bechgaard salts [61], is strongly suppressed. In effect, the triplet SCp_x superconductivity, which has a gap order parameter $\Delta_r = r\Delta$ with $r = \text{sign}\, k_x$, is an intrachain pairing that is subjected to the strongest repulsive part of the oscillating potential produced by SDW correlations [50]. More favorable conditions for triplet pairing do exist but they take place at higher angular momentum, in the interchain f-wave channel with a order parameter $\Delta_r(k_\perp) = r\Delta \cos k_\perp$, a possibility that was shown to come out from the renormalization group theory when, besides intrachain repulsive interactions, weak interchain Coulomb interactions are included [56, 57].

Appendix

1 Renormalization group approach to the one-dimensional electron gas model

In this appendix, we derive the one-loop flow equations of the one-dimensional electron gas model. This is carried out by the Kadanoff-Wilson renormalization group procedure. The partition function $Z = \mathrm{Tr}\, e^{-\beta H}$ for the electron gas model Hamiltonian is beforehand expressed in terms as functional integral over the anticommuting fermion fields ψ

$$\begin{aligned} Z &= \iint \mathcal{D}\psi^*\mathcal{D}\psi\ e^{S_0[\psi^*,\psi]+S_I[\psi^*,\psi]} \\ &= \iint \mathcal{D}\psi^*\mathcal{D}\psi\ \exp\Big\{\sum_{\widetilde{k},\alpha}[G_p^0(\widetilde{k})]^{-1}\psi^*_{p,\alpha}(\widetilde{k})\psi_{p,\alpha}(\widetilde{k}) \\ &+ \pi v_F T/L \sum_{\{\widetilde{k},\widetilde{q},\alpha\}} \tilde{g}_{\{\alpha\}}\ \psi^*_{+,\alpha_1}(\widetilde{k}_1+\widetilde{q})\psi^*_{-,\alpha_2}(\widetilde{k}_2-\widetilde{q})\psi_{-,\alpha_3}(\widetilde{k}_2)\psi_{+,\alpha_4}(\widetilde{k}_1) \\ &- \pi v_F\ T/2L \sum_{\{p,\widetilde{k},\widetilde{q},\alpha\}} \tilde{g}_3\ \psi^*_{p,\alpha}(\widetilde{k}_1+p\widetilde{q})\psi^*_{p,\alpha'}(\widetilde{k}_2-p\widetilde{q}+p\tilde{G})\psi_{-p,\alpha'}(\widetilde{k}_2)\psi_{-p,\alpha}(\widetilde{k}_1)\Big\} \end{aligned} \tag{35}$$

where

$$G_p^0(\tilde{k}) = [i\omega_n - \epsilon_p(k)]^{-1} \tag{36}$$

is the bare electron propagator for the $p = \pm$ branches, and $\tilde{k} = (k, \omega_n = \pm\pi T, \pm 3\pi T..)$. For backward and forward scattering (Fig. 18), we have defined

$$\tilde{g}_{\{\alpha\}} = \tilde{g}_1\delta_{\alpha_1\alpha_3}\delta_{\alpha_2\alpha_4} - \tilde{g}_2\delta_{\alpha_1\alpha_4}\delta_{\alpha_2\alpha_3}. \tag{37}$$

The action can then be parameterized by

$$\mu = (G_p^0, g_1, g_2, g_3). \tag{38}$$

The idea behind the Kadanoff-Wilson renormalization group is the transformation or renormalization of the action S following successive partial integration of $\bar{\psi}$'s of momentum located in the energy shell $\frac{1}{2}E_0(\ell)d\ell$ on both sides of the Fermi level, where $E_0(\ell) = E_0e^{-\ell}$ is the effective bandwidth at step ℓ of integration and $d\ell \ll 1$. The transformation of S from ℓ to $\ell + d\ell$, that keeps the partition function invariant is usually written as

$$\begin{aligned} Z = &\quad e^{A(\ell)} \iint_< \mathcal{D}\psi^*\mathcal{D}\psi e^{S[\psi^*,\psi]_<} \iint \mathcal{D}\bar{\psi}^*\mathcal{D}\bar{\psi}\, e^{S[\psi^*,\psi,\bar{\psi}^*,\bar{\psi}]_{d\ell}} \\ = &\quad e^{A(\ell+d\ell)} \iint_< \mathcal{D}\psi^*\mathcal{D}\psi e^{S[\psi^*,\psi]_{\ell+d\ell}}, \end{aligned} \tag{39}$$

where $A(\ell)$ corresponds to the free energy density at the step ℓ. The integration measure in the outer shell is

$$\mathcal{D}\bar{\psi}^*\mathcal{D}\bar{\psi} = \prod_{p,\alpha,\{\widetilde{k}\}'} d\bar{\psi}^*_{p,\alpha}(\widetilde{k})d\bar{\psi}_{p,\alpha}(\widetilde{k}). \tag{40}$$

and $\{\widetilde{k}\}' = \{k\}'\{\omega_n\}$. Here $\{k\}'$ corresponds to the momentum outer shells

$$k_0e^{-\ell} + k_F > k > k_0e^{-\ell-d\ell} + k_F \qquad (-k_0e^{-\ell-d\ell} - k_F > k > -k_0e^{-\ell} - k_F)$$

above the Fermi level and

$$-k_0e^{-\ell-d\ell} + k_F > k > -k_0e^{-\ell} + k_F \qquad (+k_0e^{-\ell} - k_F > k > +k_0e^{-\ell-d\ell} - k_F)$$

below for right (left) moving fermions, while $\{\omega_n\}$ covers all the Matsubara frequencies. The remaining inner shell $(<)$ fermion degrees of freedom are kept fixed.

In practice, the partial integration (39) is most easily performed with the aid of diagrams. We first decompose the $\widetilde{k}$ sums in the action into outer and inner shells momentum variables

$$\sum_{\{\widetilde{k}\}} = \sum_{\{\widetilde{k}\}'} + \sum_{\{\widetilde{k}\}_<} . \tag{41}$$

This allows us to write

$$S[\psi^*,\psi] = S[\psi^*,\psi]_< + S[\psi^*,\psi,\bar{\psi}^*,\bar{\psi}] \tag{42}$$

where $S[\psi^*,\psi]_<$ of the action with all the ψ's in the inner shell, whereas

$$S[\psi^*,\psi,\bar{\psi}^*,\bar{\psi}] = S_0[\bar{\psi}^*,\bar{\psi}] + S_{I,1}[\psi^*,\psi,\bar{\psi}^*,\bar{\psi}] + S_{I,2}[\psi^*,\psi,\bar{\psi}^*,\bar{\psi}] + \dots \tag{43}$$

consists in a free part in the outer momentum shell and an interacting part as a sum of terms, $S_{I,i}$, having $i = 1,\dots 4$ $\bar{\psi}'$s in the outer momentum shell. Their integration following the partial trace operation (39) is performed perturbatively with respect to $S_0[\bar{\psi}^*,\bar{\psi}]$. At the one-loop level for the interactions, only $S_{I,2}$ matters. Making use of the linked cluster theorem, the outer shell integration becomes

$$\begin{aligned} Z &= e^{A(\ell)} \iint_< \mathcal{D}\psi^*\mathcal{D}\psi e^{S[\psi^*,\psi]_<} \iint \mathcal{D}\bar{\psi}^*\mathcal{D}\bar{\psi}\, e^{S_0[\bar{\psi}^*,\bar{\psi}]} \exp\Big\{ S_{I,2}[\psi^*,\psi,\bar{\psi}^*,\bar{\psi}] + \dots \Big\} \\ &= e^{A(\ell)} \iint_< \mathcal{D}\psi^*\mathcal{D}\psi \exp\Big\{ S[\psi^*,\psi]_< + \frac{1}{2}\langle (S_{I,2})^2\rangle_{\bar{0},c} + \dots \Big\} \end{aligned} \tag{44}$$

where

$$\langle ....\rangle_{\bar{0},c} = Z_{\bar{0}}^{-1} \iint \mathcal{D}\bar{\psi}^*\mathcal{D}\bar{\psi}\, (.....)\, e^{S_0[\bar{\psi}^*,\bar{\psi}]} \tag{45}$$

is a free fermion average corresponding to a connected diagram evaluated in the outer momentum shell and

$$Z_{\bar{0}} = \iint \mathcal{D}\bar{\psi}^*\mathcal{D}\bar{\psi}\, e^{S_0[\bar{\psi}^*,\bar{\psi}]}, \tag{46}$$

is the outer shell contribution to the free partition function.

The one-loop outer-shell averages $\frac{1}{2}\langle (S_{I,2})^2\rangle$, consists of diagrams (single loops) in the Cooper and Peierls scattering channels contributing to the renormalization of coupling constants and then to their flows as a function of ℓ. More explicitely, consider the contributions of $S_{I,2}$ in the C and P channels for normal and Umklapp processes (disregarding other non singular terms), we can write schematically

$$\begin{aligned} S_{I,2}[\psi^*,\psi,\bar{\psi}^*,\bar{\psi}] \quad &= \quad S^C_{I,2} + S^P_{I,2} + S^{P,U}_{I,2} + \dots \\ &\Longleftrightarrow \quad (\bar{\psi}^*_+\bar{\psi}^*_-\psi_-\psi_+ + \text{c.c}) + (\bar{\psi}^*_+\psi^*_-\bar{\psi}_-\psi_+ + \text{c.c}) \\ &\quad + (\,\bar{\psi}^*_+\psi^*_+\bar{\psi}_-\psi_- + \psi^*_+\bar{\psi}^*_+\psi_-\bar{\psi}_- + \text{c.c}\,) \end{aligned} \tag{47}$$

This leads to

$$\frac{1}{2}\langle (S_{I,2})^2\rangle_{\bar{0},c} = \frac{1}{2}\langle (S^P_{I,2})^2\rangle_{\bar{0},c} + \frac{1}{2}\langle (S^C_{I,2})^2\rangle_{\bar{0},c} + \frac{1}{2}\langle (S^{P,U}_{I,2})^2\rangle_{\bar{0},c} + \langle S^P_{I,2}S^{P,U}_{I,2}\rangle_{\bar{0},c} \tag{48}$$

For the normal one-loop Peierls contribution, we get

$$\begin{aligned} \frac{1}{2}\langle (S^P_{I,2})^2\rangle_{\bar{0},c} \quad &= \quad \frac{T^2}{L^2}(\pi v_F)^2 \sum_{\{\tilde{k},\tilde{q},\alpha\}} \sum_{\{\tilde{k}',\tilde{q}',\alpha'\}} \tilde{g}_{\{\alpha\}}\tilde{g}_{\{\alpha'\}}\, \langle \bar{\psi}^*_+\psi^*_-\bar{\psi}_-\psi_+\psi'^*_+\bar{\psi}'^*_-\psi'_-\bar{\psi}'_+\rangle_{\bar{0},c} \\ &= \quad \frac{T^2}{L^2}(\pi v_F)^2 \sum_{\{\tilde{k},\tilde{q},\alpha\}} \sum_{\{\tilde{k}',\tilde{q}',\alpha'\}} \tilde{g}_{\{\alpha\}}\tilde{g}_{\{\alpha'\}}\, \langle \bar{\psi}^*_+\bar{\psi}_-\bar{\psi}'^*_-\bar{\psi}'_+\rangle_{\bar{0},c}\psi^*_-\psi_+\psi'^*_+\psi'_- \\ &= \Big|_{\text{Wick}} \quad \frac{T^2}{L^2}(\pi v_F)^2 \sum_{\{\tilde{k},\tilde{q},\alpha\}} \sum_{\{\tilde{k}',\tilde{q}',\alpha'\}} \tilde{g}_{\{\alpha\}}\tilde{g}_{\{\alpha'\}}\, \langle \bar{\psi}^*_+\bar{\psi}'_+\rangle_{\bar{0}}\langle \bar{\psi}'^*_-\bar{\psi}_-\rangle_{\bar{0}}\psi'^*_+\psi^*_-\psi'_-\psi_+ \end{aligned}$$

$$= \frac{T}{L}\pi v_F \sum_{\{\tilde{k}_1,\tilde{k'}_2,\tilde{q}\}}\sum_{\{\alpha,\alpha'\}} \tilde{g}_{\{\alpha\}}\tilde{g}_{\{\alpha'\}}\delta_{\alpha'_4\alpha_1}\delta_{\alpha'_2\alpha_3} I_P(\tilde{q}_P) \times \psi^*_{+,\alpha'_1}(\tilde{k'}_1+\tilde{q})\psi^*_{-,\alpha_2}(\tilde{k}_2-\tilde{q})\psi_{-,\alpha'_3}(\tilde{k'}_2)\psi_{\alpha_4}(\tilde{k}_1), \quad (49)$$

where

$$I_P(\tilde{q}_P;d\ell) = \pi v_F \frac{T}{L}\sum_k\sum_{\omega_n} G^0_+(\tilde{k})G^0_-(\tilde{k}-\tilde{q}_p) \quad (50)$$

Here the Peierls outer shell contribution will be evaluated at 'zero' *external* variables, that is for $\tilde{q}_P=(2k_F,0)$ in the Peierls channel. After the fermion frequency summation, we get

$$\begin{aligned} I_P(d\ell) &= -\frac{1}{4}\left\{\int_{-\frac{1}{2}E_0(\ell)}^{-\frac{1}{2}E_0(\ell+d\ell)} + \int_{\frac{1}{2}E_0(\ell+d\ell)}^{\frac{1}{2}E_0(\ell)}\right\}\frac{\tanh\frac{1}{2}\beta x}{x}\,dx. \\ &\simeq -\frac{1}{2}d\ell \end{aligned} \quad (51)$$

Similarly for the Cooper channel, we have

$$\begin{aligned} \frac{1}{2}\langle(S^C_{I,2})^2\rangle_{\bar{0},c} &= \frac{T^2}{L^2}(\pi v_F)^2\sum_{\{\tilde{k},\tilde{q},\alpha\}}\sum_{\{\tilde{k}',\tilde{q}',\alpha'\}}\tilde{g}_{\{\alpha\}}\tilde{g}_{\{\alpha'\}}\,\langle\bar{\psi}^*_+\bar{\psi}^*_-\psi_-\psi_+\psi'^*_+\psi'^*_-\bar{\psi}'_-\bar{\psi}'_+\rangle_{\bar{0},c} \\ &= \frac{T^2}{L^2}(\pi v_F)^2\sum_{\{\tilde{k},\tilde{q},\alpha\}}\sum_{\{\tilde{k}',\tilde{q}',\alpha'\}}\tilde{g}_{\{\alpha\}}\tilde{g}_{\{\alpha'\}}\,\langle\bar{\psi}^*_+\bar{\psi}^*_-\bar{\psi}'_-\bar{\psi}'_+\rangle_{\bar{0},c}\psi_-\psi_+\psi'^*_+\psi'^*_- \\ &= \Big|_{\text{Wick}} \frac{T^2}{L^2}(\pi v_F)^2\sum_{\{\tilde{k},\tilde{q},\alpha\}}\sum_{\{\tilde{k}',\tilde{q}',\alpha'\}}\tilde{g}_{\{\alpha\}}\tilde{g}_{\{\alpha'\}}\,\langle\bar{\psi}^*_+\bar{\psi}'_+\rangle_{\bar{0},c}\langle\bar{\psi}^*_-\bar{\psi}'_-\rangle_{\bar{0},c}\psi'^*_+\psi'^*_-\psi_-\psi_+ \\ &= \frac{T}{L}(\pi v_F)\sum_{\{\tilde{k}_{1,2},\tilde{q}\}}\sum_{\{\alpha,\alpha'\}}\tilde{g}_{\{\alpha\}}\tilde{g}_{\{\alpha'\}}\delta_{\alpha_1,\alpha'_4}\delta_{\alpha_2,\alpha'_3}\,I_C(\widetilde{q}_C;d\ell) \\ &\quad\times\psi'^*_{+,\alpha'_2}(\widetilde{k}_1+\widetilde{q})\psi'^*_{-,\alpha'_1}(\widetilde{k}_2-\widetilde{q})\psi_{-,\alpha_3}(\widetilde{k}_2)\psi_{+,\alpha_4}(\widetilde{k}_1) \end{aligned} \quad (52)$$

where

$$I_C(\widetilde{q}_C;d\ell) = \pi v_F\frac{T}{L}\sum_k\sum_{\omega_n}G^0_+(k+q_c,\omega_n+\omega_{mC})G^0_-(-k,-\omega_n). \quad (53)$$

The evaluation at zero external Cooper variable $\widetilde{q}_C=0$ and the properties $\epsilon_+(k)=\epsilon_-(-k)$ allows us to show that it reduces to the one in (51) for the Peierls channel

$$\begin{aligned} I_C(\widetilde{q}_C=0;d\ell) &= -I_P(d\ell) \\ &= \frac{1}{2}d\ell. \end{aligned} \quad (54)$$

The procedure can be carried on for the Umklapp terms with the results

$$\begin{aligned} \frac{1}{2}\langle(S^{P,U}_{I,2})^2\rangle_{\bar{0},c} &= \frac{T}{L}\pi v_F\,\tilde{g}_3^2 I_P(d\ell)\sum_{\{\tilde{k}_1,\tilde{k}_2,\tilde{q}\}}\sum_{\{\alpha,\alpha'\}}\psi^*_{+,\alpha'}(\tilde{k}_1+\tilde{q})\psi^*_{-,\alpha}(\tilde{k}_2-\tilde{q})\psi_{-,\alpha}(\tilde{k}_2)\psi_{+,\alpha'}(\tilde{k}_1) \\ \langle S^P_{I,2}S^{P,U}_{I,2}\rangle_{\bar{0},c} &= \frac{T}{L}\pi v_F\,\tilde{g}_3(2\tilde{g}_2-\tilde{g}_1)I_P(d\ell)\sum_{\{\tilde{k}_1,\tilde{k}_2,\tilde{q}\}}\sum_{\{\alpha,\alpha'\}}\psi^*_{p,\alpha}(\widetilde{k}_1+p\widetilde{q})\psi^*_{p,\alpha'}(\widetilde{k}_2-p\widetilde{q}+p\tilde{G}) \\ &\quad\times\psi_{-p,\alpha'}(\widetilde{k}_2)\psi_{-p,\alpha}(\widetilde{k}_1) \end{aligned} \quad (55)$$

where the first term contributes to $\tilde{g}_2$ while the second for $\tilde{g}_3$. Collecting all the terms yields after all cancellations the recursion relations (Fig. 23)

$$\tilde{g}_1(\ell+d\ell) = \tilde{g}_1(\ell)+2\tilde{g}_1^2(\ell)I_P(d\ell),$$

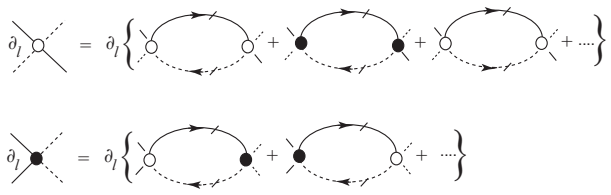

FIGURE 23. .

$$\begin{aligned}\tilde{g}_2(\ell+d\ell) &= \tilde{g}_2(\ell) - \tilde{g}_1^2 I_C(d\ell) - \tilde{g}_3^2(\ell) I_P(d\ell),\\ \tilde{g}_3(\ell+d\ell) &= \tilde{g}_3(\ell) - 2\big(2\tilde{g}_2 - \tilde{g}_1\big)(\ell)\tilde{g}_3(\ell) I_P(d\ell).\end{aligned} \tag{56}$$

, which corresponds to the RG transformation in the parameter space

$$\mathcal{R}_{d\ell}\mu(\ell) = \big(G_p^0, g_1(\ell+d\ell), g_2(\ell+d\ell), g_3(\ell+d\ell)\big). \tag{57}$$

The coupling constants are then governed by the flow equations

$$\begin{aligned}\tilde{g}_1' &= -\tilde{g}_1^2,\\ (2\tilde{g}_2 - \tilde{g}_1)' &= \tilde{g}_3^2,\\ \tilde{g}_3' &= \tilde{g}_3(2\tilde{g}_2 - \tilde{g}_1),\end{aligned} \tag{58}$$

An important feature of these equations is the fact that the flow of g_1 is entirely uncoupled from the one of $2g_2 - g_1$. This feature, which follows from the interference between the Cooper and the Peierls channels, gives rise to an important property of 1D interacting fermion systems, namely the separation of long wavelength spin and charge degrees of freedom. This is rendered manifest by rewriting the interacting part of the action as follows[35]

$$S_I[\psi^*,\psi]_\ell = -\pi v_F(2g_2 - g_1)\sum_{p,\widetilde{q}} \rho_p(\widetilde{q})\rho_{-p}(-\widetilde{q}) + \pi v_F\, g_1(\ell)\sum_{p,\widetilde{q}} \mathbf{S}_p(\widetilde{q})\cdot\mathbf{S}_{-p}(-\widetilde{q}) \tag{59}$$

where the long-wave length particle-density and spin-density fields of branch p are defined by

$$\begin{aligned}\rho_p(\widetilde{q}) &= \frac{1}{2}\sqrt{\frac{T}{L}}\sum_{\alpha,\{\widetilde{k}\}_<} \psi_{p,\alpha}^*(\widetilde{k}+\widetilde{q})\psi_{p,\alpha}(\widetilde{k})\\ \mathbf{S}_p(\widetilde{q}) &= \frac{1}{2}\sqrt{\frac{T}{L}}\sum_{\alpha,\{\widetilde{k}\}_<} \psi_{p,\alpha}^*(\widetilde{k}+\widetilde{q})\,\vec{\sigma}^{\alpha\beta}\,\psi_{p,\beta}(\widetilde{k}).\end{aligned} \tag{60}$$

The spin-charge separation is preserved at higher order and is a key property of a Luttinger liquid in one dimension [62].

Books and review articles

- *Interacting Electrons In Quasi-One-Dimensional Organic Superconductors*, Edited by A. Lebed, Springer (March 2008).

- Special volume of *Chemical Review,* **104**, (2004).

- C. Bourbonnais, *Electronic phases of low dimensional conductors,* Proc. of the international summer school on *Trends in High Magnetic Fields Science*, Edited by C. Berthier, P. Boebinger, L. P. Levy and G. Martinez, 37 pages (Springer 2002), p. 235-270 (arXiv. cond-mat/0204345).

- C. Bourbonnais and D. Jérome, *The normal phase of quasi-one-dimensional organic superconductors* , Advances in Synthetic Metals: twenty years of science and technology, Edited by P. Bernier and S. Lefrant and G. Bidan, Elsevier (1999), P. 207-261.(arXiv. cond-mat/9903101)

Renormalization group method in low dimensional materials

– C. Bourbonnais and L. G. Caron, Int. Journ. Mod. Phys. B **6**, 1033 (1991).

– C. Bourbonnais, B. Guay, and R. Wortis *Renormalization group method for quasi-one-dimensional interacting fermion systems at finite temperature*, David Snchal, Andr-Marie Tremblay and Claude Bourbonnais (eds.), Theoretical Methods for Strongly Correlated Electrons, CRM Series in Mathematical Physics, P. 75-137, Springer, New York, 2003.(arXiv. cond-mat/0204163)

– C. Bourbonnais, *Electronic phases of low dimensional conductors,* Proc. of the international summer school on *Trends in High Magnetic Fields Science*, Cargse, France, May 2001, Edited by C. Berthier, P. Boebinger, L. P. Levy and G. Martinez, 37 pages (Springer 2002), p. 235-270 (arXiv. cond-mat/0204345).

2 References

[1] H. Tanaka *et al.*, Science **291**, 285 (2001).

[2] D. S. Acker *et al.*, J. Am. Chem. Soc. **82**, 6408 (1960).

[3] F. Wudl, G. M. Smith, and E. J. Hufnagel, J. Chem. Soc., Chem. Comm. **1**, 1453 (1970).

[4] S. Yasuzuka, K. Murata, T. Arimoto, and R. Kato, J. Phys. Soc. Jpn **76**, 033701 (2007).

[5] J. P. Ferraris and T. F. Finnegan, Solid State Comm. **18**, 1169 (1976).

[6] R. Peierls, *Quantum Theory of Solids* (Oxford University Press, London, 1955), p.108.

[7] M. Meneghetti, A. Toffoletti, and L. Pasimeni, Phys. Rev. B **54**, 16353 (1996).

[8] B. Horovitz, H. Gutfreund, and M. Weger, Phys. Rev. B **12**, 3174 (1975).

[9] R. H. Friend, M. Miljak, and D. Jérome, Phys. Rev. Lett. **40**, 1048 (1978).

[10] J. Andersen *et al.*, Acta Cryst. B **34**, 1901 (1978).

[11] C. S. Jacobsen, K. Mortensen, J. R. Andersen, and K. Bechgaard, Phys. Rev. B **18**, 905 (1978).

[12] K. Bechgaard, D. O. Cowan, and A. N. Bloch, Journal of the Chemical Society, Chem. Comm. **22**, 937 (1974).

[13] J. P. Pouget, Chemica Scripta **55**, 85 (1981).

[14] A. Andrieux, C. Duroure, D. Jérome, and K. Bechgaard, J. Phys. (Paris) Lett. **40**, 381 (1979).

[15] K. Bechgaard *et al.*, Solid State Comm. **33**, 1119 (1980).

[16] P. Wzietek *et al.*, J. Phys. I **3**, 171 (1993).

[17] D. Jérome, A. Mazaud, M. Ribault, and K. Bechgaard, J. Phys. (Paris) Lett. **41**, L95 (1980).

[18] R. Brusetti, M. Ribault, D. Jerome, and K. Bechgaard, J. Phys. (Paris) **43**, 801 (1982).

[19] K. Bechgaard, M. Carneiro, M. Olsen, and F. Rasmussen, Phys. Rev. Lett. **46**, 852 (1981).

[20] D. L. Pévelen *et al.*, Eur. Phys. J. B **19**, 363 (2001).

[21] G. Brun *et al.*, C.R. Acad. Sc. (Paris) **284 C**, 211 (1977).

[22] S. Flandrois *et al.*, Mol. Cryst. Liq. Cryst. **79**, 307 (1982).

[23] C. Coulon *et al.*, J. Phys. (Paris) **43**, 1059 (1982).

[24] L. Ducasse *et al.*, J. Phys. C **19**, 3805 (1986).

[25] D. Chow *et al.*, Phys. Rev. Lett. **81**, 3984 (1998).

[26] B. J. Klemme *et al.*, Phys. Rev. Lett. **75**, 2408 (1995).

[27] L. Balicas *et al.*, J. Phys. I (France) **4**, 1539 (1994).

[28] D. Jaccard *et al.*, J. Phys.: Cond. Matt. **13**, 89 (2001).

[29] T. Adachi *et al.*, J. Am. Chem. Soc. **122**, 3238 (2000).

[30] M. Itoi *et al.*, J. Phys. Soc. Japan **76**, 053703 (2007).

[31] M. Itoi *et al.*, J. Phys. Soc. Japan **76**, 053703 (2007).

[32] P. Auban-Senzier *et al.*, Synthetic Metals **133-134**, 11 (2003).

[33] D. Jaccard *et al.,* unpublished data (2008).

[34] Y. A. Bychkov, L. P. Gorkov, and I. Dzyaloshinskii, Sov. Phys. JETP **23**, 489 (1966).

[35] I. E. Dzyaloshinskii and A. I. Larkin, Sov. Phys. JETP **34**, 422 (1972).

[36] J. Solyom, Adv. Phys. **28**, 201 (1979).

[37] S. Barisic and S. Brazovskii, in *Recent Developments in Condensed Matter Physics*, edited by J. T. Devreese (Plenum, New York, 1981), Vol. 1, p. 327.

[38] V. J. Emery, R. Bruisma, and S. Barisic, Phys. Rev. Lett. **48**, 1039 (1982).

[39] V. J. Emery, in *Highly Conducting One-Dimensional Solids*, edited by J. T. Devreese, R. E. Evrard, and V. E. van Doren (Plenum, New York, 1979), p. 247.

[40] T. Giamarchi, *Quantum Physics in One Dimension* (Oxford University Press, Oxford, 2004).

[41] C. Bourbonnais and L. G. Caron, Int. J. Mod. Phys. B **5**, 1033 (1991).

[42] C. Bourbonnais, in *Trends in High Magnetic Fields Science*, edited by L. P. L. C. Berthier, P. Boebinger and G. Martinez (Springer, Heidelberg, 2002), arXiv. cond-mat/0204345.

[43] L. P. Gor'kov and I. E. Dzyaloshinskii, JETP Lett. **18**, 401 (1973).

[44] C. Bourbonnais, J. Phys. I (France) **3**, 143 (1993).

[45] M. Kimura, Prog. Theor. Phys. **63**, 955 (1975).

[46] J. Voit, Eur. Phys. J. B **5**, 505 (1998).

[47] C. Bourbonnais and D. Jérome, Science **281**, 1156 (1998).

[48] W. Kohn and J. M. Luttinger, Phys. Rev. Lett. **15**, 524 (1965).

[49] V. J. Emery, Synthetic Metals **13**, 21 (1986).

[50] M. T. Béal-Monod, C. Bourbonnais, and V. J. Emery, Phys. Rev. B **34**, 7716 (1986).

[51] L. G. Caron and C. Bourbonnais, Physica **143B**, 453 (1986).

[52] C. Bourbonnais and L. G. Caron, Europhys. Lett. **5**, 209 (1988).

[53] D. J. Scalapino, E. Loh, and J. E. Hirsch, Phys. Rev. B **34**, R8190 (1986).

[54] H. Shimahara, J. Phys. Soc. Jpn. **58**, 1735 (1989).

[55] H. Kino and H. Kontani, J. Phys. Soc. Jpn. **68**, 1481 (1999).

[56] J. C. Nickel, R. Duprat, C. Bourbonnais, and N. Dupuis, Phys. Rev. Lett. **95**, 247001 (2005).

[57] J. C. Nickel, R. Duprat, C. Bourbonnais, and N. Dupuis, Phys. Rev. B **73**, 165126 (2006).

[58] R. Duprat and C. Bourbonnais, Eur. Phys. J. B **21**, 219 (2001).

[59] C. Bourbonnais and R. Duprat, J. de Phys. IV **114**, 3 (2004).

[60] Y. Fuseya and Y. Suzumura, J. Phys. Soc. Jpn. **74**, 1263 (2005).

[61] A. G. Lebed, K. Machida, and M. Ozaki, Phys. Rev. B **62**, R795 (2000).

[62] F. D. M. Haldane, J. Phys. C **14**, 2585 (1981).